



RESEARCH ARTICLE

Reprogramming of T cell-derived small extracellular vesicles using IL2 surface engineering induces potent anti-cancer effects through miRNA delivery

Dokyung Jung¹  | Sanghee Shin²  | Sung-Min Kang¹ | Inseong Jung²  |
 Suyeon Ryu¹ | Soojeong Noh² | Sung-Jin Choi² | Jongwon Jeong² | Beom Yong Lee² |
 Kwang-Soo Kim² | Christine Seulki Kim² | Jong Hyuk Yoon⁴ | Chan-Hyeong Lee¹ |
 Felicitas Bucher⁵ | Yong-Nyun Kim⁶ | Sin-Hyeong Im^{7,8,9} | Byoung-Joon Song¹⁰ |
 Kyungmoo Yea^{2,3} | Moon-Chang Baek¹ 

¹Department of Molecular Medicine, CMRI, Exosome Convergence Research Center (ECRC), School of Medicine, Kyungpook National University, Daegu, Republic of Korea

²Department of New Biology, DGIST, Daegu, Republic of Korea

³New Biology Research Center, DGIST, Daegu, Republic of Korea

⁴Department of Neural Development and Disease, Korea Brain Research Institute, Daegu, Republic of Korea

⁵Eye Center, Medical Center, Faculty of Medicine, University of Freiburg, Freiburg, Germany

⁶Division of Translational Science, National Cancer Center 323, Ilsan-ro, Ilsandong-gu, Goyang-si, Gyeonggi-do, Republic of Korea

⁷Department of Life Sciences, Pohang University of Science and Technology (POSTECH), Gyeongsangbuk-do, Republic of Korea

⁸Institute of Convergence Science, Yonsei University, Seoul, Republic of Korea

⁹ImmunoBiome, Pohang, Republic of Korea

¹⁰Section of Molecular Pharmacology and Toxicology, Laboratory of Membrane Biochemistry and Biophysics, National Institute on Alcohol Abuse and Alcoholism (NIAAA), Bethesda, Maryland, USA

Correspondence

Moon-Chang Baek, Department of Molecular Medicine, CMRI, Exosome Convergence Research Center (ECRC), School of Medicine, Kyungpook National University, Daegu, 41944, Republic of Korea.

Email: mcbaek@knu.ac.kr

Kyungmoo Yea, Department of New Biology, DGIST, Daegu, 43024, Republic of Korea.

Email: ykm31@dgist.ac.kr

Funding information

Ministry of Science and ICT, South Korea, Grant/Award Numbers: 2017M3A9G8083382, 2019M3A9H1I03607, 2020M3A9I4039539, 2021R1A5A2021614, 21-DGRIP-01, NCC-2032052020; Joint Research Project of Institutes of Science and Technology

Abstract

T cell-derived small extracellular vesicles (sEVs) exhibit anti-cancer effects. However, their anti-cancer potential should be reinforced to enhance clinical applicability. Herein, we generated interleukin-2-tethered sEVs (IL2-sEVs) from engineered Jurkat T cells expressing IL2 at the plasma membrane via a flexible linker to induce an autocrine effect. IL2-sEVs increased the anti-cancer ability of CD8⁺ T cells without affecting regulatory T (T_{reg}) cells and down-regulated cellular and exosomal PD-L1 expression in melanoma cells, causing their increased sensitivity to CD8⁺ T cell-mediated cytotoxicity. Its effect on CD8⁺ T and melanoma cells was mediated by several IL2-sEV-resident microRNAs (miRNAs), whose expressions were upregulated by the autocrine effects of IL2. Among the miRNAs, miR-181a-3p and miR-223-3p notably reduced the PD-L1 protein levels in melanoma cells. Interestingly, miR-181a-3p increased the activity of CD8⁺ T cells while suppressing T_{reg} cell activity. IL2-sEVs inhibited tumour progression in melanoma-bearing immunocompetent mice, but not in immunodeficient mice. The combination of IL2-sEVs and

Moon-Chang Baek and Kyungmoo Yea contributed equally to this work.

This is an open access article under the terms of the [Creative Commons Attribution-NonCommercial-NoDerivs License](https://creativecommons.org/licenses/by-nc-nd/4.0/), which permits use and distribution in any medium, provided the original work is properly cited, the use is non-commercial and no modifications or adaptations are made.

© 2022 The Authors. *Journal of Extracellular Vesicles* published by Wiley Periodicals, LLC on behalf of the International Society for Extracellular Vesicles.

existing anti-cancer drugs significantly improved anti-cancer efficacy by decreasing PD-L1 expression in vivo. Thus, IL2-sEVs are potential cancer immunotherapeutic agents that regulate both immune and cancer cells by reprogramming miRNA levels.

KEYWORDS

cancer, exosomal PD-L1, interleukin-2, PD-L1, small extracellular vesicle, small extracellular vesicle engineering

1 | INTRODUCTION

Small extracellular vesicles (sEVs) are nanoparticles released by most cells (They et al., 2002) and carry various bioactive molecules (proteins, lipids, metabolites, and nucleic acids) responsible for cell-to-cell communication in multicellular organisms (El et al., 2013; Wiklander et al., 2019). Compared to conventional nanoparticles such as viral and synthetic nanocarriers, endogenously derived sEVs can evade phagocytosis, retain high biocompatibility, and exhibit low immunogenicity (Cheng et al., 2018; Wang et al., 2020). Importantly, sEVs can be engineered to acquire therapeutic potential and enhance the efficacy of existing agents (Herrmann et al., 2021; Wiklander et al., 2019). Considering these unique and beneficial characteristics, sEVs have recently attracted considerable attention in the field of nanoparticle-based therapeutics in many areas, including anti-cancer treatment.

Cancer cells release sEVs to evade immune surveillance, and conversely, immune cells release sEVs to control tumour progression (Marar et al., 2021; Yan & Jiang, 2020). Cancer cell-derived sEVs (CA-sEVs) can make the tumour microenvironment favourable for tumour progression and metastasis (Kaiser, 2016; Peinado et al., 2012). According to recent studies, CA-sEVs express programmed cell death ligand-1 (PD-L1) in the same surface topology as that of the parent cells. CA-sEVs with PD-L1, that is exosomal PD-L1 (ePD-L1) is considered an important means for cancer immune escape, which involves inhibition of T cell activity, eventually leading to tumour progression (Poggio et al., 2019; Xie et al., 2019). Interestingly, ePD-L1 causes resistance against immune checkpoint therapy by directly binding to programmed cell death protein 1 (PD-1) of CD8⁺ T cells, thereby inhibiting their cytotoxic effects on cancer cells. In addition, high levels of ePD-L1 can neutralize the action of anti-PD-1/PD-L1 antibodies (α PD-1/PD-L1 Ab) (Poggio et al., 2019; Xie et al., 2019). Therefore, suppression of ePD-L1 level or sEV secretion by cancer cells can be a strong anti-cancer strategy to overcome resistance to current α PD-1/PD-L1 Ab therapy.

Recent studies have revealed that immune cell-derived sEVs (IM-sEVs) play an important role in the immune system by stimulating the immunomodulatory actions of immune cells (Mittal et al., 2020; Torralba et al., 2018). IM-sEVs are involved in crosstalk between innate and adaptive immunity (Yan & Jiang, 2020). Reports have revealed that similar to parental dendritic cells (DCs), DC-derived sEVs increase the antigen-specific response of T cells by presenting MHC-peptide complexes to T cells (Pitt et al., 2014). sEVs released by CD8⁺ T cells can deplete mesenchymal stem cells in tumour tissue, preventing tumour invasion and metastasis (Seo et al., 2018). In addition, CD4⁺ T cell-derived sEVs can activate B cells to enhance the antigen-specific humoral immune response (Lu et al., 2019). Collectively, IM-sEVs can perform immunomodulatory functions targeting cancer cells and are considered an alternative for cancer immunotherapy. However, the anti-cancer potential of T cell-derived sEVs should be improved to enhance its clinical applicability. Therefore, manipulating IM-sEVs to increase or expand their function may further enhance their immunotherapeutic efficacy against cancer.

In this study, we aimed to generate interleukin-2-tethered T cell sEVs (IL2-sEVs) from engineered T cells by attaching IL2 to the cell surface using a flexible linker (Figure 1A). IL2-sEVs exerted an anti-cancer effect by inducing CD8⁺ T cell-mediated cytotoxicity without affecting regulatory T (T_{reg}) cell activity. Self-stimulation of T cells by membrane-bound IL2 changed the microRNA (miRNA) profile of sEVs, which lowered PD-L1 expression and sEV secretion by cancer cells, resulting in elevated anti-cancer effects. Furthermore, in mouse melanoma models, IL2-sEVs potently inhibited both tumour growth and metastasis while it also improved anti-cancer efficacy in combination with known anti-cancer agents. We propose that reprogramming of IM-sEVs by cytokine tethering may be a powerful method for increasing the beneficial cargo of sEVs, thereby acting as an improved cancer immunotherapeutic that modulates both cancer and immune cells.

2 | RESULTS

2.1 | IL2-sEVs induced CD8⁺ T cell proliferation and activation without affecting the T_{reg} cells

IL2 is known to exert anti-cancer effects on melanoma and kidney cancer (Jiang et al., 2016; Spolski et al., 2018). Recently, reports have revealed that IM-sEVs, including T cell-derived sEVs, suppress tumour progression (Wang et al., 2020; Yan & Jiang, 2020; Torralba et al., 2018; Seo et al., 2018). Based on these reports, we developed a new strategy to generate a potent anti-cancer agent by combining IL2, a key immune-stimulating factor, with T cell-derived sEVs possessing anti-cancer properties. Previously, we have

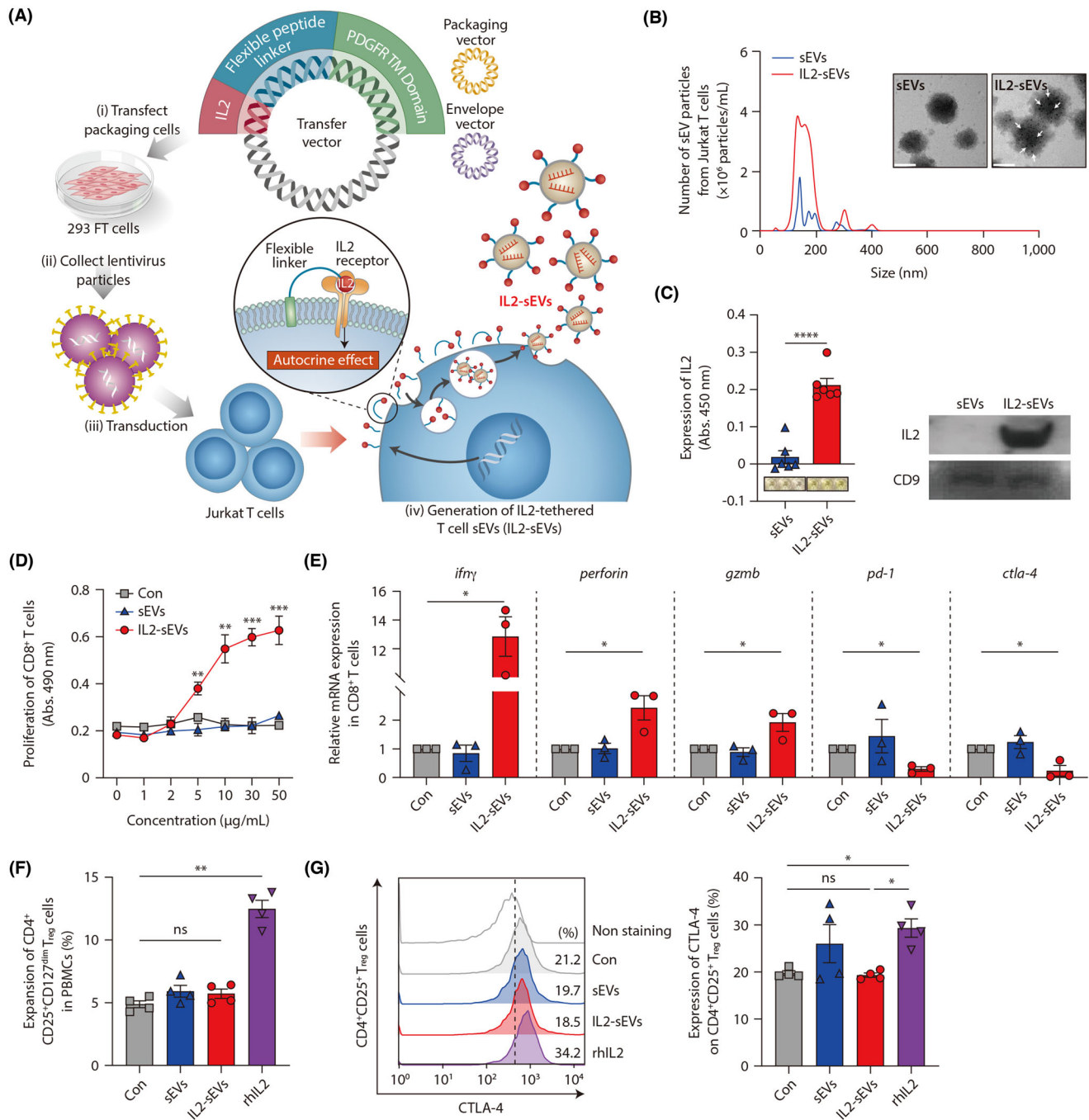


FIGURE 1 Generation of IL2-sEVs and their function in T cells. (A) Schematic illustration of the production of IL2-sEVs. IL2 was attached to the transmembrane domain (TM) of platelet-derived growth factor receptor (PDGFR) via a flexible linker and then this gene was incorporated into lentiviruses for Jurkat T cell infection. Infected Jurkat T cells secrete IL2-sEVs. (B) Size distribution and representative images of sEVs and IL2-sEVs measured using nanoparticle tracking analysis (NTA) and TEM. TEM image of IL2-sEVs bound to antibody-linked gold nanoparticles, demonstrating the attachment of IL2 to the sEV. White arrows in the black-boxed inset indicate IL2 on the IL2-sEV surface. Scale bars, 100 nm. (C) Detection of IL2 on IL2-sEVs using ELISA (left, $n = 6$) and western blotting (right). (D) The dose-dependent effect of PBS (Con), sEVs, or IL2-sEVs on the proliferation of CD8⁺ T cells was measured using the MTS assay ($n = 3$). Data indicate mean \pm SEM. ** $p < 0.01$, *** $p < 0.001$ versus Con. (E) Expression of activation markers for CD8⁺ T cells after treatment with PBS, sEVs (10 μ g), or IL2-sEVs (10 μ g). mRNA levels of *interferon- γ* (*ifn γ*), *perforin*, *granzyme b* (*gzmb*), *pd-1*, and *ctla-4* were determined by quantitative real-time PCR (qRT-PCR) ($n = 3$). (F) Expansion of CD4⁺, CD25⁺, CD127^{dim} T_{reg} cells from human PBMCs after treatment with PBS, sEVs (10 μ g), IL2-sEVs (10 μ g), or rhIL2 (200 IU) was measured using flow cytometry ($n = 4$). (G) Representative flow cytometric histograms (left) and bar graphs (right) indicate activity of isolated CD4⁺, CD25⁺ T_{reg} cells after treatment with PBS, sEVs (10 μ g), IL2-sEVs (10 μ g), or rhIL2 (200 IU) ($n = 4$). Data represent mean \pm SEM. * $p < 0.05$, ** $p < 0.01$, *** $p < 0.001$, **** $p < 0.0001$, and ns, not significant using the Student's t-test in (C), comparison among indicated groups using one-way ANOVA combined with the post-hoc Dunnett test for (E) to (G), and comparison among indicated groups using two-way ANOVA combined with the post-hoc Tukey for (D).

developed a method where membrane-tethered cytokines function in an autocrine manner (Bucher et al., 2018; Zha et al., 2017). Cytokine-tethered sEVs derived from T cells can be generated using this method (Figure 1A). Here, we engineered Jurkat T cells that displayed IL2 on their surface via a flexible peptide linker (Figure 1A and Figures S1A–C) (Bucher et al., 2018; Zha et al., 2017). This membrane-linked IL2 is non-diffusive and stimulates recipient cells in an autocrine manner (Figure 1A). IL2-sEVs were harvested and characterized from the culture medium of the engineered T cells. The physical characteristics of sEVs, including the size and level of IL2 expression, were verified (Figures 1B, C and Figures S1D–G) (Im et al., 2019; Xu et al., 2015). Transmission electron microscopy (TEM) analysis revealed the morphology of IL2-sEVs with an average diameter of about 150 nm. In addition, TEM analysis confirmed IL2 attachment to the sEV surface after labelling the antibody-linked gold nanoparticles (Figure 1B). Enzyme-linked immunosorbent assay (ELISA) and immunoblotting further verified that IL2 was tethered on the sEV surface (Figure 1C and Figures S1F, G). Interestingly, IL2 tethering considerably enhanced sEV secretion from T cells compared to that from the control (Figure 1B and Figure S1D). Next, we checked the immuno-modulating effects of IL2-sEVs on T cells, including CD8⁺ T cells and T_{reg} cells. The MTS assay revealed that CD8⁺ T cell proliferation significantly increased following IL2-sEV treatment than in the control (Figure 1D). Additionally, IL2-sEV treatment significantly increased the mRNA expression of CD8⁺ T cell activation markers, including IFN- γ , perforin, and granzyme B, while decreasing the expression of immune checkpoints, such as PD-1 and CTLA-4 (Figure 1E). Remarkably, when peripheral blood mononuclear cells (PBMCs) were treated with sEVs or IL2-sEVs, the T_{reg} cell population was not affected, unlike that observed after recombinant human IL2 (rhIL2) treatment (Figures 1F, G and Figure S1H).

2.2 | Membrane-bound IL2 partially contributed to the immune-stimulatory function of IL2-sEVs

As cytokines attached to the cell surface via a flexible linker can stimulate the cells themselves (Bucher et al., 2018; Zha et al., 2017), we wondered whether the internal contents of sEVs were also affected by autocrine stimulation of IL2 during IL2-sEV production. Furthermore, we investigated whether the altered internal contents conferred potent anti-cancer effects of IL2-sEVs. As expected, IL2-mediated CD8⁺ T cell proliferation and activation were completely blocked by treatment with anti-IL2 antibody (α IL2 Ab) (Figures 2A and B). Surprisingly, however, α IL2 Ab treatment only partially inhibited the IL2-sEV-mediated regulation of CD8⁺ T cells (Figures 2A, B and Figures S2A, B). When we tested the efficiency of immune cell-mediated melanoma killing following IL2-sEV treatment in an in vitro co-culture assay, immune cell-mediated cancer cell death after IL2-sEV treatment was significantly higher than that after PBS or sEV treatment (Figures 2C–H). Intriguingly, α IL2 Ab treatment only slightly inhibited cancer cell death by IL2-sEVs (Figures 2C–H). Based on these findings, we hypothesized that the autocrine IL2 signalling on Jurkat T cells altered the internal contents of IL2-sEVs, inducing the anti-cancer effects of IL2-sEVs.

2.3 | miRNAs enriched in IL2-sEVs potentially down-regulated both cellular and ePD-L1 levels in melanoma cells and suppressed T_{reg} cell activity

To identify the altered payload of IL2-sEVs responsible for their anti-cancer activity, we performed proteomic analysis (Cho et al., 2017; Moon et al., 2011) and miRNA-sequencing (miRseq) analysis (Cheng et al., 2014; Huang et al., 2013) of IL2-sEVs. Compared to that observed for sEVs, proteomic analysis of IL2-sEVs did not reveal any significant changes in the protein profile related to key immunological functions (Figure S3A and Tables S1, 2). In contrast, 2588 miRNAs were detected in the miRNA profile analysis of sEVs and IL2-sEVs, where 247 IL2-sEV miRNAs were overexpressed 1.5 times more than sEV miRNAs (Figure 3A). Based on the miRseq data, further analyses, such as categorized mapping and reference studies (Kalantari Khandani et al., 2020) were performed to classify miRNAs according to their regulatory effects on immune cells and cancer cells. Among the 247 more abundant miRNAs in IL2-sEVs, 14 miRNAs related to immune stimulation (Figure S3B), seven miRNAs connected to tumour suppressor function (Figure S3C), and 11 miRNAs associated with PD-L1 regulation were identified (Figure 3A).

To confirm the efficacy of miRNAs, six most abundant miRNAs (miR-17-5p, miR-29a-3p, miR-92a-1-5p, miR-125a-5p, miR-181a-3p, and miR-223-3p) among the 14 miRNAs related to immune stimulation were selected and their ability to affect the functions of immune cells such as CD8⁺ T cells and T_{reg} cells were determined (Figure S3B). Interestingly, miRNAs such as miR-181a-3p mildly increased the expression of proliferation and activation markers of CD8⁺ T cells (Figures S4A–D). In particular, miR-29a-3p significantly reduced PD-1 expression in CD8⁺ T cells to a level similar to the changes observed after IL2-sEV treatment (Figures S2A and S4E). As IL2-sEVs did not affect T_{reg} cells unlike IL2, we studied whether the miRNAs in IL2-sEVs affected T_{reg} cells. Hence, we tested the effect of those six miRNAs on the mRNA levels of transforming growth factor (TGF)- β (Stockis et al., 2009) and cytotoxic T lymphocyte-associated antigen (CTLA)-4 (Read et al., 2000), which play important roles in T_{reg} cell activity. Interestingly, miRNAs, such as miR-181a-3p and miR-29a-3p, presented potent inhibitory effects on T_{reg} cell activity, suggesting that the T_{reg} cell stimulation by membrane-bound IL2 of IL2-sEVs is likely to be neutralized by the reprogrammed, T_{reg} cell-inhibitory miRNAs inside the sEVs (Figure S4F).

Next, we investigated the effect of miRNAs on PD-L1 regulation in melanoma cells. Six most abundant miRNAs (miR-101-3p, miR-146a-5p, miR-150-5p, miR-181a-3p, miR-200c-3p, and miR-223-3p) among the aforementioned 11 miRNAs involved

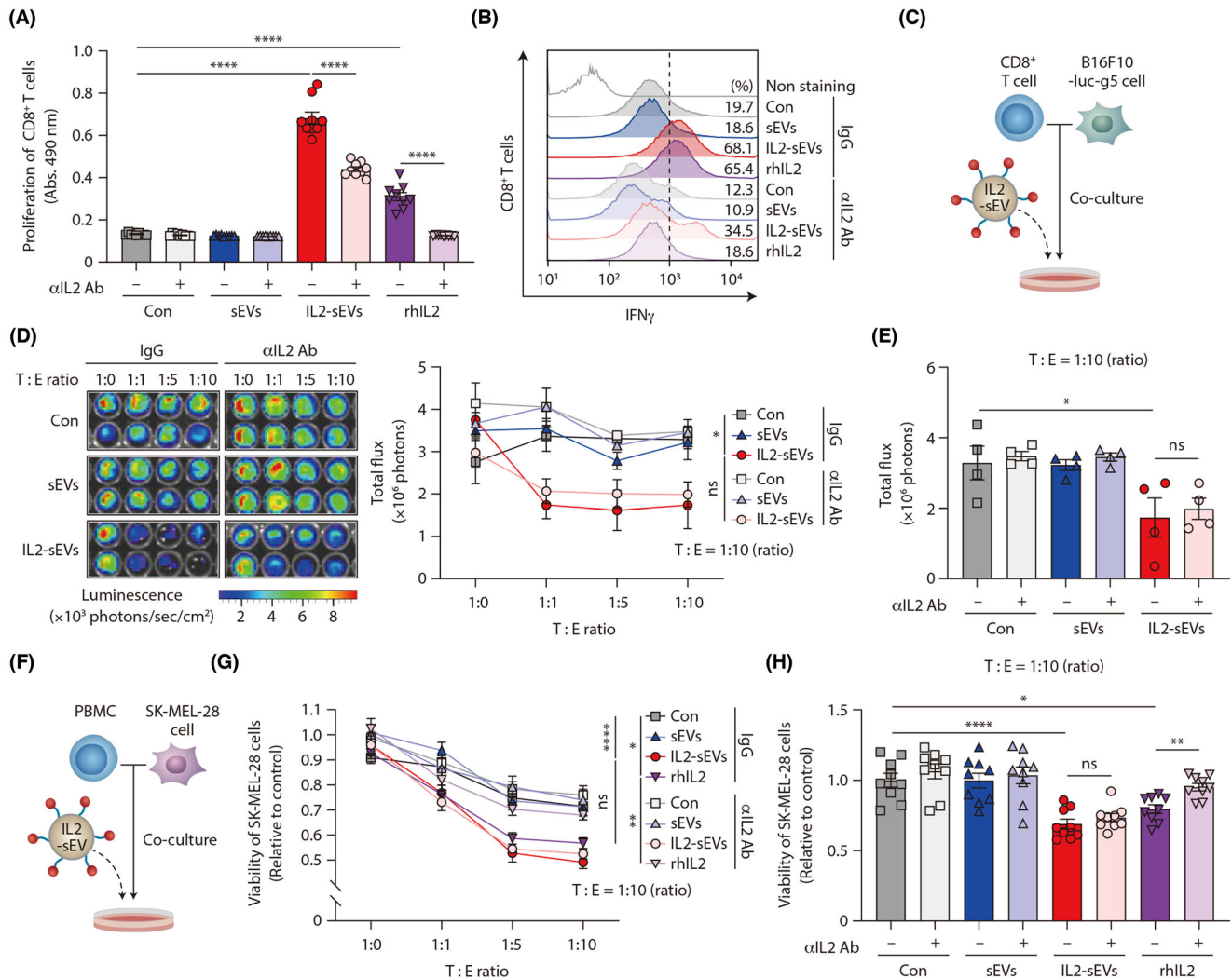


FIGURE 2 Immune stimulation by IL2-sEVs was only partially inhibited by anti-IL2 Ab (α IL2 Ab) treatment. (A and B) Proliferation and IFN- γ expression of CD8⁺ T cells were measured using the MTS assay (A) ($n = 9$) and flow cytometry (B) after treatment with PBS (Con), sEVs (10 μ g), IL2-sEVs (10 μ g), or rhIL2 (200 IU) with or without treatment with α IL2 Ab. (C–H) Effect of IL2-sEVs on effector cells [CTLL-2 (D and E) or PBMCs (G and H)]; E: effector cell-mediated cytotoxicity against melanoma cells (T: target cells) with or without treatment of α IL2 Ab. (C) and (F) Schematic diagrams of co-culture assays. Cell viability was measured using in vitro bioluminescent (D and E) or MTS assay (G and H). (D) Represents bioluminescent images and right panel indicates line plot ($n = 9$). Data represent mean \pm SEM. * $p < 0.05$ and ns, not significant versus Con. (E) Quantification of target cell viability at a T:E = 1:10 ratio ($n = 4$) from (D). (H) Target cell viability at a T:E = 1:10 ratio ($n = 9$) from (G). Data indicate mean \pm SEM. * $p < 0.05$, ** $p < 0.01$, **** $p < 0.0001$, and ns, not significant versus Con. E and T represent effector cells and target cells, respectively. Data represent mean \pm SEM. * $p < 0.05$, ** $p < 0.01$, **** $p < 0.0001$, and ns, not significant in comparison among different groups using two-way ANOVA combined with the post-hoc Tukey for (A), (D), (E), (G), and (H)

in PD-L1 regulation were selected to evaluate their effects on PD-L1 mRNA expression in melanoma cells (Figures 3A and B). Among them, three miRNAs (miR-101-3p, miR-181a-3p, and miR-223-3p) significantly reduced the mRNA level of PD-L1 by about 30% compared to that in the control group (Figure 3B). In addition, miR-181a-3p and miR-223-3p significantly decreased the protein level of PD-L1 in human melanoma cells by more than 40% compared to that in the control groups (Figure 3C). Based on the results of miRNA experiments, we evaluated whether IL2-sEVs regulated PD-L1 expression as active miRNAs. Western blot analysis showed that IL2-sEVs significantly inhibited PD-L1 expression in melanoma cells, which was also confirmed using immunocytochemistry (Figures 3D–F). In addition to cellular PD-L1, IL2-sEVs notably reduced the expression of ePD-L1 in melanoma cells (Figures 3G–I). Next, we co-cultured IL2-sEV-pretreated melanoma cells with CD8⁺ T cells to determine whether melanoma cells with PD-L1 suppression became more sensitive to the cytotoxic effects of CD8⁺ T cells. The melanoma cells pretreated with IL2-sEVs presented a 35.9% increase in cancer cell death compared to that in the PBS-treated cells (Figures 3J–L). Taken together, our data suggest that the IL2-sEV-mediated reduction in cellular and ePD-L1 in melanoma cells may contribute to the efficacy of CD8⁺ T cell-mediated killing of cancer cells. Furthermore, the anti-cancer effect of IL2-sEVs may be mediated by both surface IL2 and internal miRNAs such as miR-181a-3p.

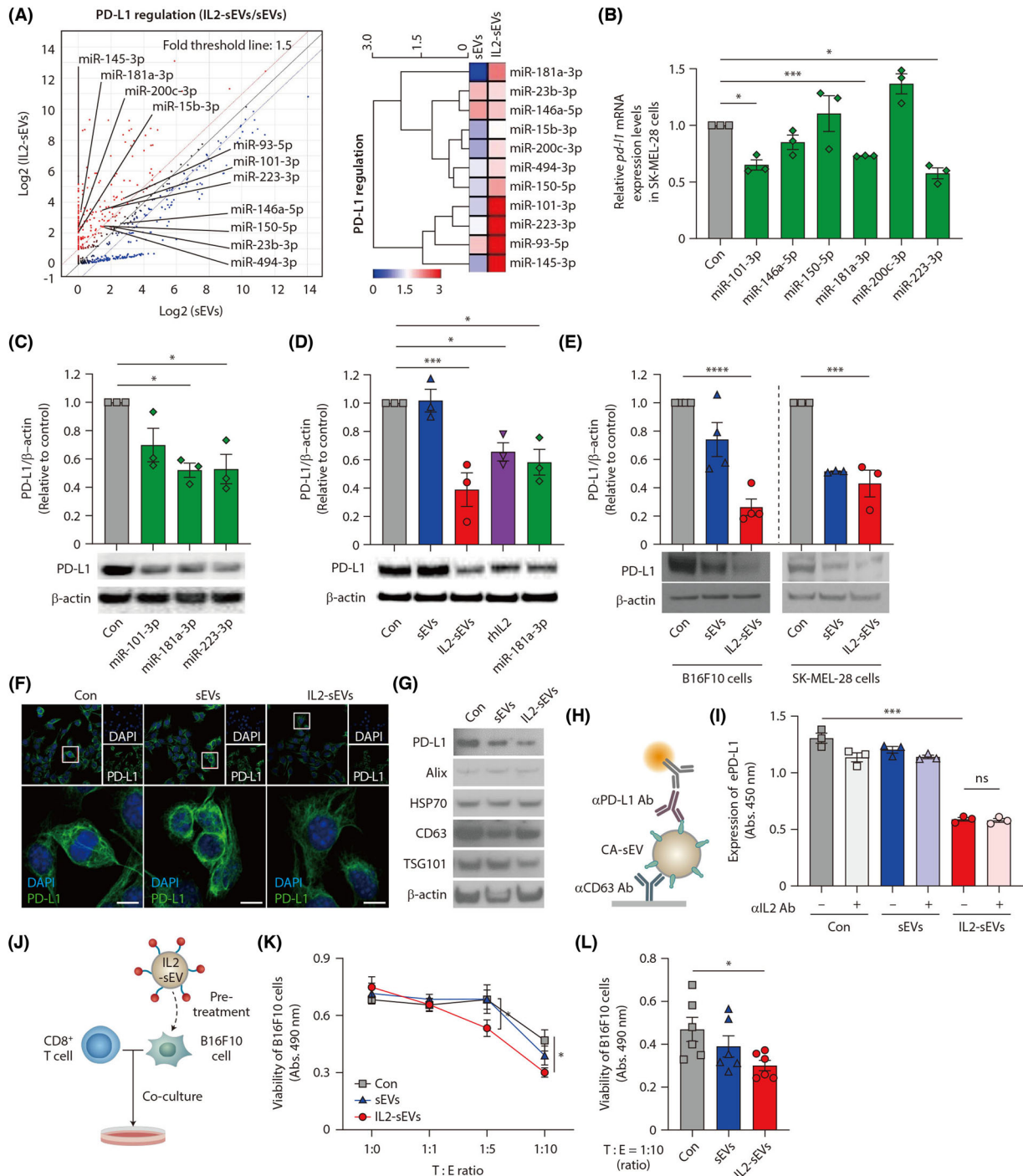


FIGURE 3 IL2-sEV-derived miRNAs lowered PD-L1 levels in melanoma cells. (A) Scatter plot (left) and heat map (right) indicate changes in expression of miRNAs regulating PD-L1 after exposure to sEVs or IL2-sEVs. Each experiment was performed twice and all measurements were averaged. (B) Relative mRNA levels of the PD-L1 in SK-MEL-28 cells 24 h post-transfection with each miRNA candidate ($n = 3$). (C and D) Western blot analysis of PD-L1 protein expression in SK-MEL-28 cells ($n = 3$) after miRNA transfection or treatment with PBS (Con), sEVs, IL2-sEVs, or rhIL2. (E) The protein level of PD-L1 was measured in both mouse (B16F10) and human (SK-MEL-28) melanoma cells using western blotting after treatment with PBS, sEVs (10 μg), or IL2-sEVs (10 μg) ($n = 3-4$). (F) Representative images of immunofluorescent PD-L1 staining (green) in B16F10 cells after treatment with PBS, sEVs (10 μg), or IL2-sEVs (10 μg). Scale bars, 10 μm. (G) Western blot analysis for PD-L1 expression in melanoma cell-derived sEVs after treatment with PBS, sEVs (10 μg), or IL2-sEVs (10 μg). (H) Schematic diagram of ELISA for quantification of ePD-L1. (I) ePD-L1 levels in melanoma cells were measured after treatment with PBS, sEVs (10 μg), or IL2-sEVs (10 μg) in the presence or absence of αIL2 Ab ($n = 3$). (J) Schematic illustration of co-culture assays. (K and L) B16F10 cells were pretreated with PBS, sEVs (10 μg), or IL2-sEVs (10 μg). (K) Viability of B16F10 cells in this assay at different CD8⁺ T cell ratio ($n = 6$). Data indicate mean ± SEM. * $p < 0.05$ versus Con. (L) Quantification of target cell viability at a T:E = 1:10 ratio ($n = 6$) from (K). Data are represented by mean ± SEM. * $p < 0.05$, *** $p < 0.001$, **** $p < 0.0001$, and ns, not significant in comparison among different groups using one-way ANOVA combined with the post-hoc Dunnett test for (B-E) and (L), and comparison among indicated groups using two-way ANOVA combined with the post-hoc Tukey for (I) and (K)

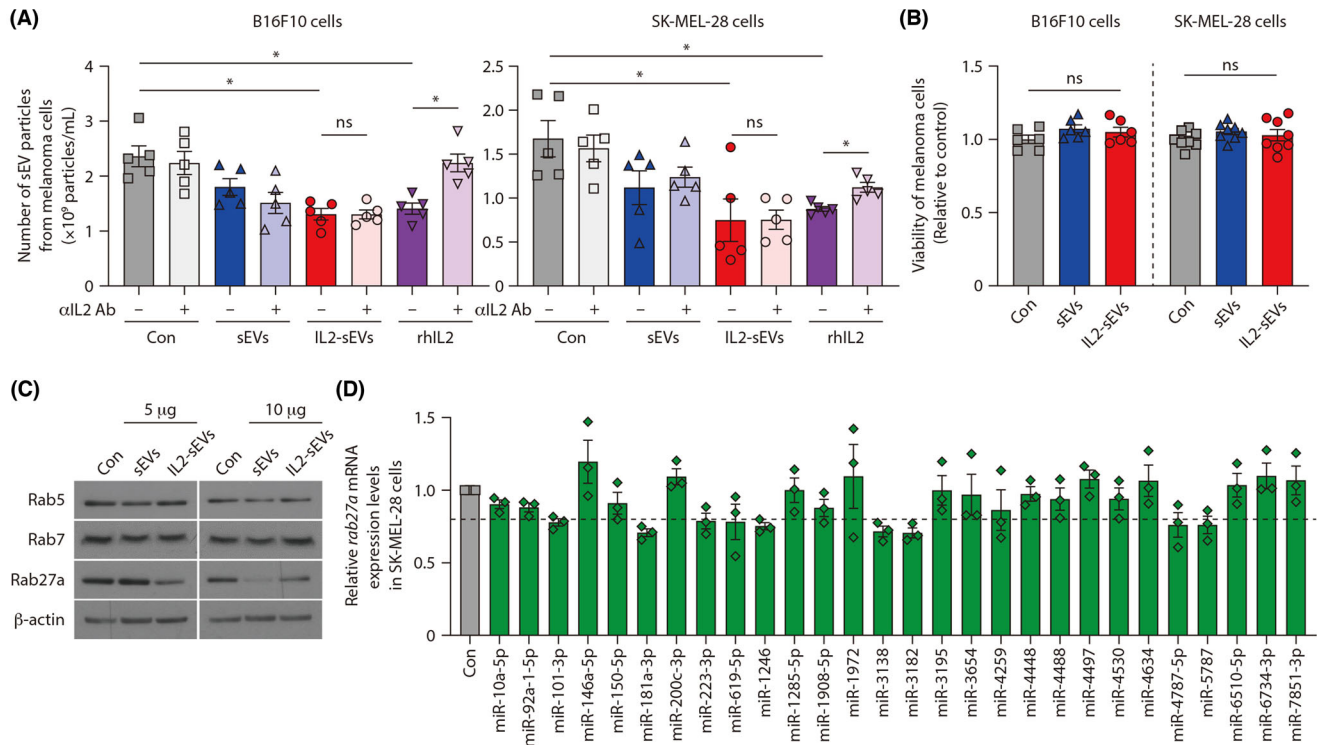


FIGURE 4 IL2-sEVs and their miRNAs suppressed sEV secretion in melanoma cells. (A) Quantification of sEV particles from PBS (Con), sEV (10 μ g), IL2-sEV (10 μ g), or rhIL2 (200 IU)-treated mouse and human melanoma cells with or without treatment with α IL2 Ab using NTA ($n = 5$). (B) The viability of mouse and human melanoma cells was measured using the MTS assay after treatment with PBS, sEVs (10 μ g), or IL2-sEVs (10 μ g) ($n = 6-8$). (C) Inhibition of Rab GTPases after treatment with two different doses of IL2-sEVs. (D) Relative mRNA levels of Rab27a in SK-MEL-28 cells at 24 h post-transfection with miRNAs ($n = 3$). The black dotted line indicates 20% inhibition of Rab27a mRNA expression versus Con. Data represent mean \pm SEM. * $p < 0.05$, and ns, not significant in comparison among indicated groups using one-way ANOVA combined with the post-hoc Dunnett test for (B) and (D), and comparison among indicated groups using two-way ANOVA combined with the post-hoc Tukey for (A)

2.4 | miRNAs enriched in IL2-sEVs suppressed sEV secretion in melanoma cells

As CA-sEVs contribute to tumour development and progression, suppression of sEV secretion by cancer cells, including inhibition of PD-L1 expression, could be a powerful anti-cancer strategy (Bobrie et al., 2012; Datta et al., 2017; Im et al., 2019; Poggio et al., 2019; Xie et al., 2019). To test whether IL2-sEVs can regulate sEV secretion by cancer cells, mouse or human melanoma cells were exposed to PBS, sEVs, IL2-sEVs, or rhIL2 for 48 h after pretreatment with a control IgG or α IL2 Ab. Interestingly, treatment with either IL2-sEVs or rhIL2 significantly reduced the release of CA-sEVs without affecting the viability of melanoma cells (Figures 4A and B). However, unlike that observed with rhIL2, the inhibition of CA-sEV release by IL2-sEVs was not completely overcome by treatment with α IL2 Ab (Figure 4A). In line with the reduction in CA-sEV secretion after IL2-sEV treatment, the expression of Rab GTPases involved in the regulation of sEV secretion (Bobrie et al., 2012; Im et al., 2019; Poggio et al., 2019; Zerial & McBride, 2001) was decreased in IL2-sEV-treated melanoma cells. In particular, IL2-sEVs down-regulated the expression of Rab27a, a key regulator of the sEV transport system (Figure 4C). To determine whether the miRNAs of IL2-sEVs were related to the sEV secretion of cancer cells, we investigated the effect of miRNAs on the expression of Rab27a in melanoma cells. The expression of Rab27a mRNA transcript was measured after exposure of human melanoma cells to each one of the 28 miRNAs. Among the 28 miRNAs mentioned above, nine miRNAs tended to decrease the mRNA level of Rab27a by around 20% compared to that of the control (Figure 4D). Collectively, IL2-sEVs exhibited anti-cancer efficacy by directly suppressing cancer cells, specifically by inhibiting their secretion of sEVs and PD-L1 expression.

2.5 | IL2-sEVs induced potent anti-cancer effects in vivo

Based on our in vitro data, we next investigated the anti-cancer efficacy of IL2-sEVs in vivo using a syngeneic mouse model of melanoma. We administered control PBS, sEVs, IL2-sEVs, or rhIL2 intratumourally after 5 days of subcutaneous injection of B16F10-luc-g5 cells into wild type (WT) C57BL/6 mice. IL2-sEVs significantly inhibited tumour growth and relieved symptoms of splenomegaly more effectively than sEVs or rhIL2 (Figures 5A, B and Figures S5A, B). To confirm whether the regulatory effects

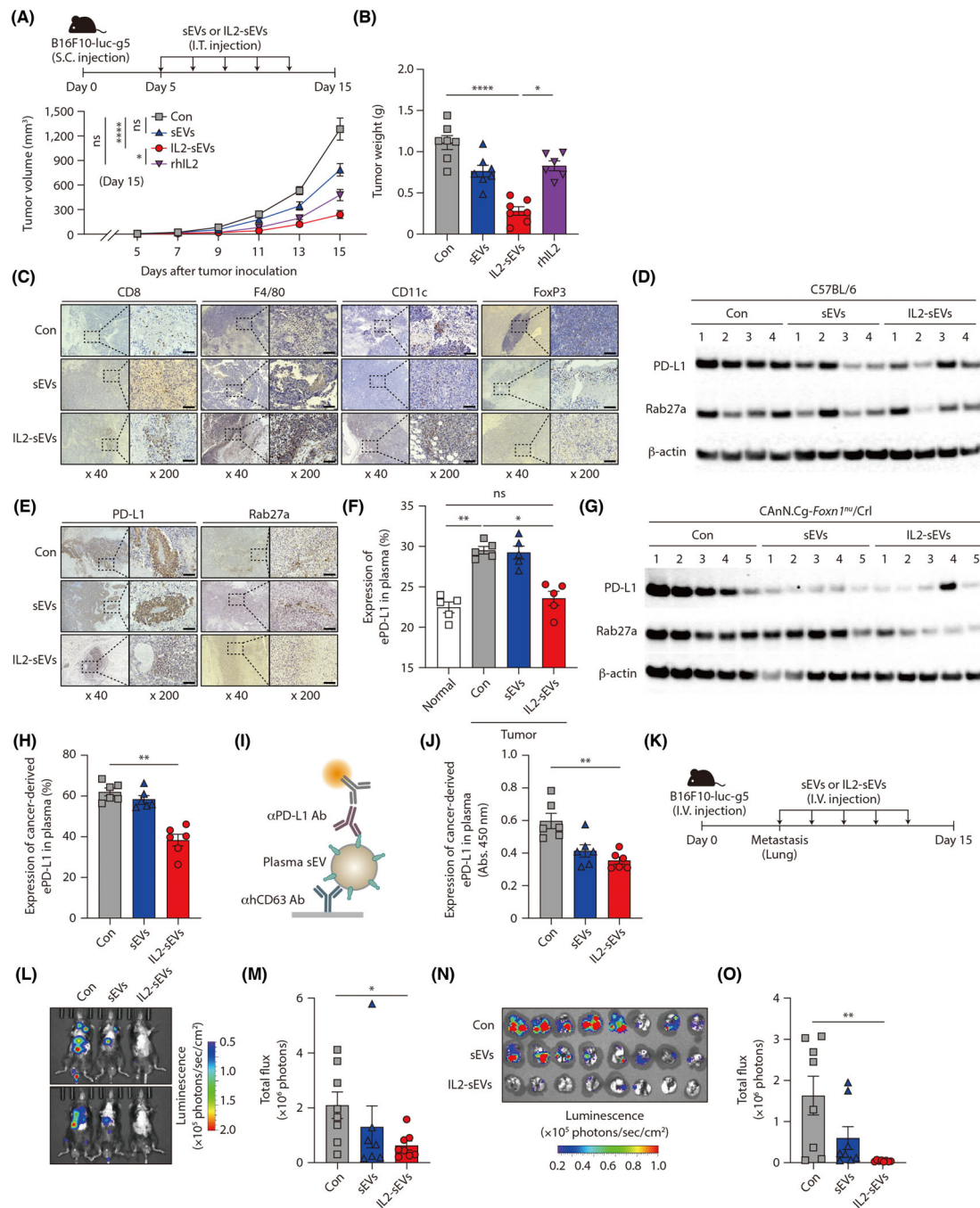


FIGURE 5 Anti-cancer effect of IL2-sEVs in melanoma mouse models. (A–F) B16F10-luc-g5 cells were subcutaneously injected into WT C57BL/6 mice. Five days after cancer cell injection, PBS (Con), sEVs (20 μg), IL2-sEVs (20 μg), or rhIL2 (50,000 IU) were administered intratumorally. (A) The therapeutic design (top) and tumour volumes of allografts in WT C57BL/6 mice (bottom; mean ± SEM) ($n = 6-7$ /group). (B) Weight of excised tumours from each group ($n = 6-7$ mice/group). (C) Immunohistochemistry (IHC) analysis of the tumour tissues of each group that showed infiltration of immune cells (CD8: cytotoxic T cells, F4/80: macrophages, CD11c: DCs, and FoxP3: T_{reg} cells). Scale bars, 100 μm. (D) Western blot analysis of PD-L1 and Rab27a expression in tumour tissues. (E) IHC analysis of PD-L1 and Rab27a expression in tumour tissues for each group. Scale bars, 100 μm. (F) Flow cytometry for ePD-L1 level in plasma from normal and tumour-bearing mice ($n = 5$ mice/group). (G–J) SK-MEL-28 cells were subcutaneously injected into CAnN.Cg-Foxn1tm/Crl mice. (G) Western blot analysis of PD-L1 and Rab27a expression in tumour tissues. (H) The expression of plasma ePD-L1 derived from cancer cells was determined using flow cytometry ($n = 6$ mice/group). (I) Schematic diagram of (J) analysis. (J) ELISA to determine the level of cancer-derived ePD-L1 in plasma ($n = 6$ mice/group). (K–O), WT C57BL/6 mice ($n = 7-8$ mice/group) were intravenously injected with B16F10-luc-g5 cells. When the pulmonary metastatic model was established, sEVs (20 μg), IL2-sEVs (20 μg), or PBS were administered via the tail vein. (K) The therapeutic design of the study. (L) Representative images and (M) total flux of in vivo bioluminescence imaging of pulmonary metastasis in each group at the day of sacrifice ($n = 6-8$). (N) Bioluminescence images and (O) total flux of melanoma cells in excised lung tissues of each group. Data represent mean ± SEM. * $p < 0.05$, ** $p < 0.01$, **** $p < 0.0001$, and ns, not significant in comparison among indicated groups using one-way ANOVA combined with the post-hoc Dunnett test for (B) and (M), and comparison among groups using Kruskal–Wallis with post-hoc Dunn’s nonparametric test for (F), (H), (J) and (O), and comparison among indicated groups using two-way ANOVA combined with the post-hoc Tukey for (A)

of IL2-sEVs on immune cells observed *in vitro* are similar to those observed in the mouse model, the immune cell population in the spleen and peripheral blood were analysed after intratumoural injection of sEVs or IL2-sEVs. Both the CD8⁺ and CD4⁺ T cell population slightly increased following IL2-sEV treatment in the spleen, whereas the T_{reg} cell population significantly decreased (Figure S5C). Furthermore, treatment with IL2-sEVs led to the recruitment of pan T cells (CD3ε⁺), CD8⁺ T cells (CD8⁺), macrophages (F4/80⁺), and DCs (CD11c⁺) to the tumour site, while the recruitment of T_{reg} cells (FoxP3⁺) was reduced (Figure 5C and Figure S5D). When analyzing the direct effect of IL2-sEVs on cancer cells *in vivo*, the expression levels of PD-L1 and Rab27a in tumour tissue also decreased in the IL2-sEV-treated group compared to that in the control groups (Figures 5D, E and Figure S5E), in agreement with the *in vitro* data. To measure the expression level of ePD-L1 in plasma, we performed bead-based sEV analysis using flow cytometry (Figure S5F). (Van Der Vlist et al., 2012) The plasma level of ePD-L1 of IL2-sEV-treated mice was significantly lower than that of tumour-bearing control mice, bringing the ePD-L1 level back to that observed in healthy control mice (Figure 5F and Figure S5G).

To further confirm that the anti-cancer efficacy of IL2-sEVs was mediated by IL2-sEV-dependent immune cell activation, human melanoma cells were injected into immunodeficient mice to generate a mouse model of melanoma xenograft. Consistent with our hypothesis, IL2-sEVs did not suppress tumour growth in immunodeficient mice unlike a melanoma syngeneic mouse model (Figures S5H and I). Importantly, the expression of both PD-L1 and Rab27a in the tumour tissue was significantly lower in the IL2-sEV-treated group than in the control group in this mouse model (Figure 5G). Furthermore, IL2-sEV injection in these immunodeficient mice significantly reduced the expression of ePD-L1 in peripheral blood, similar to that observed in the syngeneic mouse model of melanoma (Figures 5H–J).

In addition to intratumoural injection, the anti-cancer effect of IL2-sEVs was confirmed using intravenous injection, which is commonly used in the clinic. IL2-sEVs significantly reduced the size and weight of tumour even after intravenous injection in a syngeneic mouse model of melanoma (Figures S6A and B). To further investigate the effect of IL2-sEVs on cancer metastasis, a model of pulmonary metastasis was generated by intravenous injection of B16F10-luc-g5 cells into mice (Figure 5K). IL2-sEVs exhibited potent regression of tissue metastases, including to the lung, liver, bone, lymph nodes, and kidneys (Figures 5L–O and Table S3). Taken together, our *in vivo* study suggests that IL2-sEVs control both immune cells and cancer cells, which are key players in the regulation of cancer immunity and ultimately induce potent anti-cancer effects in mouse tumour models.

2.6 | Combination of IL2-sEVs with existing anti-cancer drugs enhanced the efficacy of their monotherapy

To improve the low response rate of patients with melanoma to chemotherapy (Legha et al., 1996; Pectasides et al., 1989) and immunotherapy (Cascio et al., 2021; Noman et al., 2020; Chen et al., 2018), we assessed whether IL2-sEVs could enhance the therapeutic efficacy of known anti-cancer drugs, including cisplatin (Legha et al., 1996; Pectasides et al., 1989) and αPD-L1 Ab (Cascio et al., 2021; Noman et al., 2020) in a combination therapy approach. Compared to that observed in the control group, cisplatin monotherapy inhibited tumour growth by 47.3% in a melanoma syngeneic model (Figure 6A). The combination of IL2-sEVs and cisplatin induced significant inhibitory effect compared to that observed in the cisplatin or IL2-sEV monotherapy group (Figure 6B). We also observed that the combined therapy of IL2-sEVs with cisplatin inhibited the expression of PD-L1 and Rab27a in tumour tissue to a larger extent than cisplatin monotherapy (Figure 6C). Similarly, combined treatment of IL2-sEVs with an αPD-L1 Ab drastically suppressed tumour growth and weight compared to that observed in the αPD-L1 Ab or IL2-sEV monotherapy group (Figures 6D and E). Consistently, combined treatment with cisplatin and combination therapy with αPD-L1 Ab also reduced the expression of PD-L1 and Rab27a more than αPD-L1 Ab monotherapy (Figure 6F). These data confirmed that the combination therapy of IL2-sEVs and existing anti-cancer drugs significantly improved the therapeutic potential of each monotherapy and may increase the response rate of the known cancer drugs.

3 | DISCUSSION

In this study, engineered sEVs were developed for the purpose of attaching IL2, a representative immunomodulatory cytokine, to the surface of T cell-derived sEVs to improve their original anti-cancer efficacy (Figure 1A). However, contrary to our hypothesis, sEV engineering not only conferred immune stimulatory activity of IL2 to sEVs, but also drastically changed their functional efficacy. First, sEVs released from IL2-tethered T cells changed the profile of miRNAs with immune and cancer cell regulatory functions (Figure 3A and Figures S3B, C). Therefore, it can be used as an alternative method for the cargo loading, such as the loading of miRNAs into sEVs. Second, unlike soluble IL2, IL2-sEVs induced the activation and proliferation of CD8⁺ T cells without affecting T_{reg} cells; hence, it is better than soluble IL2 as an immunotherapeutic agent (Figures 1D–G and Figures S2A, B). Finally, the stimulation of T cells by IL2 not only changed the miRNA profile of sEVs (Figure 3A and Figures S3B, C), but also increased their sEV secretion ability. IL2 signaling via surface engineering in T cells, in particular, increased sEV production by approximately 3.8-fold (Figure 1B and Figure S1D). Thus, our method can be technically utilized to augment

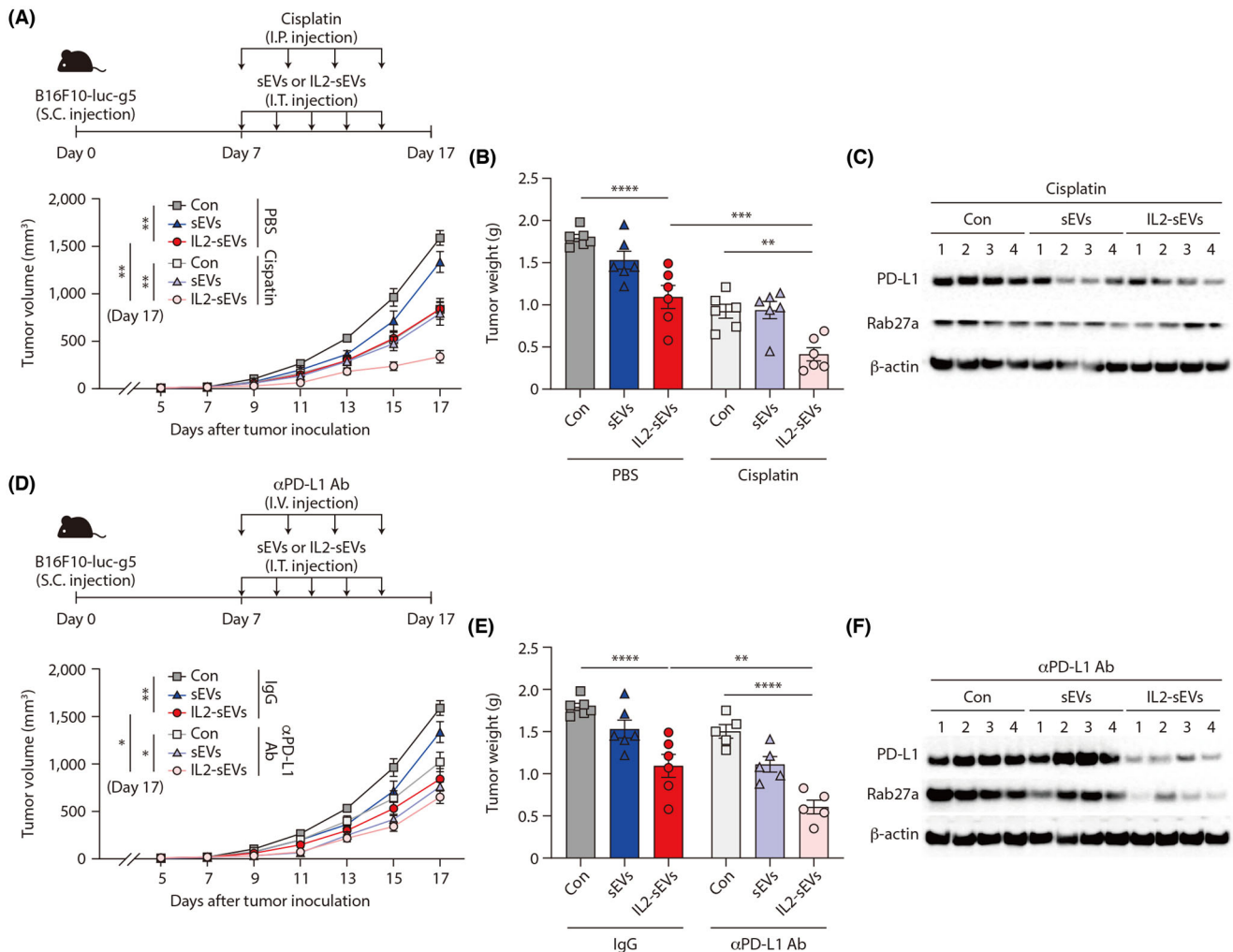


FIGURE 6 Effect of the combination of IL2-sEVs and existing anti-cancer drugs in melanoma syngeneic models. (A–F) B16F10-luc-g5 cells were subcutaneously injected into WT C57BL/6 mice. Seven days after cancer cell injection, sEVs or known anti-cancer drugs were administered intratumourally three times a week for 17 days. (A) The schematic diagram (top) and tumour volume of xenografts was measured either in monotherapy or in combination with cisplatin (bottom: mean \pm SEM). (B) Weight of excised tumours from each group ($n = 6$ mice/group). (C) Western blot analysis of PD-L1 and Rab27a in tumour tissues after combination therapy with cisplatin ($n = 4$ tumours/group). (D) The therapeutic design (top) and tumour volume of xenografts was measured either in monotherapy or in combination with α PD-L1 Ab ($n = 5$ – 6 mice/group) (bottom: mean \pm SEM). (E) Weight of excised tumours from each group ($n = 5$ – 6 mice/group). (F) Western blot analysis of PD-L1 and Rab27a in tumour tissues after combination therapy with α PD-L1 Ab. Data represent mean \pm SEM. * $p < 0.05$, ** $p < 0.01$, *** $p < 0.001$, and **** $p < 0.0001$ in comparison among groups using two-way ANOVA combined with the post-hoc Tukey for (A), (B), (D), and (E)

sEV production efficiency. Taken together, sEV surface-bound IL2 improved the anti-cancer activity of T cell sEVs and also contributed to the enhancement of sEV production by T cells, thereby increasing the clinical applicability of T cell sEVs as a superior immunotherapeutic agent.

ePD-L1 in cancer cells promotes cancer development and progression via immune evasion (Poggio et al., 2019; Xie et al., 2019). Circulating PD-L1-positive sEVs interact with PD-1 expressed on the surface of CD8⁺ T cells, leading to PD-1 signaling, which strongly suppresses T cell-mediated immune responses. Although α PD-1/PD-L1 Ab therapy has been used in a wide range of clinical settings, ePD-L1-mediated therapeutic resistance to this Ab remains challenging and this problem needs to be addressed (Poggio et al., 2019; Xie et al., 2019). In this regard, the combination of PD-L1 down-regulation and suppression of sEV secretion may be an efficient strategy to overcome the limitation of α PD-1/PD-L1 Ab therapy (Bobrie et al., 2012; Datta et al., 2017; Im et al., 2019; Poggio et al., 2019; Xie et al., 2019). So far, brefelamide analogs, such as the TPFS compounds, are the only reported PD-L1 down-regulators, although their effects are minimal (Zhang et al., 2020). Therefore, there is a strong need for the development of effective agents for inhibiting the level of ePD-L1. In this study, IL2-sEVs down-regulated the expression level of ePD-L1 and sEV secretion in both mouse and human melanoma cells (Figures 3G–I and 4A) and in mouse models (Figures 5D–J), suggesting that IL2-sEVs have the potential to be clinically used as a combination therapy to overcome resistance to checkpoint inhibitors such as α PD-1/PD-L1 Ab.

IL2 was approved for the treatment of metastatic melanoma by the Food and Drug Administration owing to its ability to mediate cancer regression (Choudhry et al., 2018; Jiang et al., 2016). However, IL2 monotherapy has not been used extensively, as IL2-mediated T_{reg} cell expansion induces unwanted immune tolerance (Ahmadzadeh & Rosenberg, 2006). In this study, we investigated whether IL2-sEVs can exert anti-cancer activity similar to IL2 monotherapy. Our results demonstrated that IL2-sEVs enhanced the proliferation and activation of $CD8^+$ T cells (Figures 1D, E, 2A and B). Contrary to IL2, IL2-sEVs did not promote T_{reg} cell expansion (Figures 1F and G). Although this effect could be attributed to differences in sEV uptake by cell type, we hypothesize that this was likely mediated by miRNAs such as miR-181a-3p within reprogrammed IL2-sEVs (Figures S4A–F). Previous studies also revealed that miRNA activates $CD8^+$ T cells while inhibiting T_{reg} cell activity (Li et al., 2007; Liu et al., 2020). The results of these investigations are consistent with our findings that miRNAs regulate cellular function differently depending on the cell type. Internally reprogrammed IL2-sEV contents, such as miRNAs, may have induced immunological activation and overcome major challenges of IL2 monotherapy, such as immunosuppression by T_{reg} cells.

CA-sEVs have generally been reported to inhibit the conversion of cold tumours, which have low immune cell infiltration, into responsive phenotypes with high immune infiltration, that is hot tumours with better prognosis (Marar et al., 2021; Sheehan & D'Souza-Schorey, 2019; Yang et al., 2020). CA-sEVs inhibit recruitment of tumour-infiltrating lymphocytes, other than T_{reg} cells, into the tumour microenvironment (Poggio et al., 2019; Sheehan & D'Souza-Schorey, 2019). In addition, CA-sEVs suppress the immune system by inducing apoptosis of $CD8^+$ T cells, reducing cytotoxicity of natural killer cells, and regulating the differentiation of DCs and macrophages (Sheehan & D'Souza-Schorey, 2019; Yang et al., 2020). Furthermore, CA-sEVs induce the proliferation of T_{reg} cells (Muller et al., 2017; Szajnik et al., 2010) and the differentiation of bone marrow-derived inhibitory cells (Peinado et al., 2012). Immunohistological profiling to analyse whether IL2-sEVs affected immune cell recruitment into cancer tissues showed that IL2-sEVs promoted accumulation of T cells, DCs, and macrophages in cancer tissues, while reducing the recruitment of T_{reg} cells (Figure 5C and Figure S5D). Therefore, a cold-to-hot tumour transition may occur following IL2-sEV treatment, contributing to the reduction in tumour volume in vivo.

Cargo loading of sEVs is an important tool for reinforcing the therapeutic efficacy of sEVs (El et al., 2013; Liang et al., 2020). Methods such as electroporation, sonication, and genetic manipulation are commonly used for cargo loading of sEVs (El et al., 2013; Liang et al., 2020; Gangadaran & Ahn, 2020; Fu et al., 2019). However, these methods have many disadvantages. In the case of electroporation for encapsulating nucleic acids, problems such as precipitation and degradation arise with size-dependent loading inefficiency; furthermore, sEVs become unstable due to undesirable zeta potential and colloidal effects. The loaded cargos are limited to small non-biological molecules in the sonication method (Gangadaran & Ahn, 2020; Luan et al., 2017). In the genetic method, the payload gene is simply overexpressed inside the parent cells and the expressed gene products are integrated into the sEVs (Cheng et al., 2018; Fu et al., 2019). Here, we attached IL2 to the surface of the sEVs using genetic engineering techniques (Figure 1A). In addition to induction of primary immune activation by membrane-bound IL2 on the sEV surface, autocrine-based IL2 stimulation in parental cells can induce dramatic enrichment of anti-cancer miRNAs inside sEVs (Figure 3A and Figures S3B–E). Therefore, compared to the previous cargo loading methods, our new, improved method may be potentially used for various therapeutic applications. In particular, cytokine-tethered IM-sEVs can be effectively applied to sEV-based cancer immunotherapy, as has been demonstrated here.

Several studies have shown that molecules attached to the surface of EVs can exert more prominent biological effects than soluble ones. For example, Koh et al. developed sEVs expressing signal regulatory protein α (SIRP α) to block the interaction between macrophage SIRP α and the innate immune checkpoint, CD47. SIRP α -exosomes showed a stronger anti-tumour effect compared to recombinant SIRP α proteins (Koh et al., 2017). Additionally, Tian et al. demonstrated that T_{reg} cell-derived sEVs, engineered to express VEGF antibody, remarkably inhibited ocular neovascularization compared to VEGF antibody alone (Tian et al., 2021). In line with previous studies, surface-engineered IL2-sEVs showed a more potent biological effect, compared to recombinant IL2. Furthermore, IL2-sEVs showed an additional advantage by an autocrine effect on surface-engineered IL2. Attaching an active cytokine, such as IL2, to the surface of immune cells would be an effective strategy for increasing the therapeutic efficacy of sEVs derived from the engineered immune cells. However, the IL2-sEVs do not have the specificity of target cells. Antibody engineering on EVs has facilitated their cell-specific delivery (Fu et al., 2019; Luan et al., 2017). Therefore, combining active cytokine engineering with antibody engineering on immune cells might improve the specificity and efficacy of the engineered EVs.

In summary, the expression of IL2 via a flexible linker on the surface of T cells induces dramatic improvements in anti-cancer miRNA contents of sEVs, in addition to the direct immune stimulation by IL2. Remarkably, these IL2-sEVs preferentially increased the proliferation and activity of $CD8^+$ T cells without affecting T_{reg} cells. Furthermore, IL2-sEVs reduced cellular and ePD-L1 levels both in vitro and in vivo melanoma models. Hence, we proposed that reprogrammed IL2-sEVs are potent cancer immunotherapeutics that work by modulating both immune and cancer cells. We anticipate that the use of IL2-sEVs alone or in combination with conventional immunotherapy may lead to significant advances in future cancer therapy. In addition, our novel method of engineering sEVs presents a considerable potential for robust reprogramming for sEV-based therapy beyond artificial payloads.

4 | MATERIALS AND METHODS

4.1 | Preparation of lentivirus

293FT cells were co-transfected with lentiviral transfer plasmids containing interleukin-2 (IL2) using the pCMVD8.9 and pVSVg viral packaging vectors in the ratio of 1:1:1. The DNA-lipofectamine complex was removed after overnight incubation and fresh medium was added to the cell culture dishes. The supernatants containing lentiviruses were harvested after 48 h and filtered through a 0.45 μm polyethersulfone membrane filter (Millipore). The lentivirus titers were determined using a Lenti-X p24 ELISA kit (Clontech).

4.2 | Tethering of IL2 to the surface of T cell sEVs

To generate IL2-tethered sEVs from Jurkat T cells, cells were infected with lentiviruses containing IL2 linked by a flexible glycine-serine linker to the transmembrane domain of platelet-derived growth factor receptor (Bucher et al., 2018; Zha et al., 2017). IL2-tethered Jurkat T cells were sorted using flow cytometry. Then, sEVs were isolated from the culture media of engineered Jurkat T cells using ultracentrifugation. Jurkat T cells were cultured in Roswell Park Memorial Institute medium (RPMI, Gibco) containing 10% fetal bovine serum (FBS, Gibco) and 1% penicillin-streptomycin (PS, Gibco).

4.3 | Cells and cell culture

B16F10, SK-MEL-28, and CTLL-2 were purchased from the American Type Culture Collection. The cells were cultured in the medium at 37°C in a humidified incubator with 5% CO₂. B16F10, B16F10-luc-g5 (Caliper), 293FT (Thermo Fisher Scientific), and HEK-blue-IL2 cells (InvivoGen) were cultured in Dulbecco's modified Eagle's medium (DMEM) containing 10% FBS and 1% PS. SK-MEL-28 cells were cultured in minimum essential medium (Gibco) containing 10% FBS and 1% PS. Jurkat T cells, CTLL-2 cells, and three types of isolated human primary cells (Peripheral blood mononuclear cells (PBMCs)) (Hokland & Heron, 1980; Romeu et al., 1992), CD8⁺ T cells, (Finney et al., 2004) and T_{reg} cells (Liu et al., 2006; Stockis et al., 2009) were cultured in RPMI medium with 10% FBS and 1% PS. Isolated healthy donor human PBMCs were collected from the Kyungpook National University Medical Center (KNUMC). Blood collection was approved by the institutional review board of KNUMC and Daegu Gyeongbuk Institute of Science & Technology (DGIST) (KNUCH 2019-09-015-005 and DGIST-20210128-BR-095-02) and written informed consent was obtained from all healthy donors.

4.4 | Isolation of sEVs

The sEVs were isolated as described previously (Im et al., 2019; Xu et al., 2015). Briefly, the individual supernatants from B16F10, SK-MEL-28, and Jurkat T cells were serially centrifuged at 300 $\times g$ for 5 min, 2500 $\times g$ for 20 min, and 10,000 $\times g$ for 30 min, respectively. The supernatants were then filtered using 0.2 μm syringe filters and centrifuged at 120,000 $\times g$ for 90 min. The purified sEV pellets were resuspended in phosphate buffered saline (PBS) or radioimmunoprecipitation assay buffer (50-188, Merck Millipore) for the experiments. (Im et al., 2019)

4.5 | TEM

The sEV pellets were fixed with 2.5% glutaraldehyde in a 0.1 M phosphate buffer. The sEV samples were deposited on pure carbon-coated EM grids. After staining with 1% uranyl acetate, the grids were dried at room temperature and viewed at $\times 12,000$ magnification using a bio-transmission electron microscope (FEI/Tecnai G2 F20 TWIN TMP, Hitachi) operated at 120 kV. IL2-sEVs were incubated with anti-Flag primary antibody for 1 h at 4°C to demonstrate the presence of IL2 on their surface using TEM. Gold nanoparticles (10 nm) labeled with goat anti-rabbit IgG secondary antibody were added and incubated for 2 h at room temperature.

4.6 | NTA

Cell culture supernatants containing sEVs were analysed using a NanoSight LM10 device. A monochromatic laser beam at 405 nm was used to analyse the nanoparticles and a video of 1 min duration was captured at the rate of 30 frames/s and camera level of 7. Approximately 50–150 particles were analysed in each field of view, and the Brownian movement of the particles was assessed using the NTA software (version 2.3, NanoSight). NTA post-acquisition settings were optimized and kept constant between samples, and the recorded video was analysed to measure particle size and concentration.

4.7 | Quantitative reverse transcription-polymerase chain reaction (qRT-PCR)

Total RNA was extracted from cells using the MiniBEST Universal RNA extraction kit (9767, TaKaRa) according to the manufacturer's protocol. Complementary strands of DNA were generated from total RNA using the PrimeScript™ 1st strand cDNA synthesis kit (6110A, TaKaRa). The qRT-PCR products were detected using the TB Green™ Premix Ex Taq™ kit (RR420A, TaKaRa). All qRT-PCR amplifications were performed in triplicate in a 20 μ l reaction volume with the indicated primer pairs. qRT-PCR was performed using a StepOnePlus qRT-PCR system (Applied Biosystems). Relative quantity of mRNA samples was calculated using comparative threshold cycle (Ct) analysis after normalization to *gapdh* mRNA levels in the same samples.

4.8 | Reporter cell assay

The HEK-Blue IL2 reporter cell assay was performed according to the protocol described by the manufacturer (hkb-il2, InvivoGen). HEK-Blue IL2 reporter cells were seeded at a density of 5×10^5 cells/ml in a 96-well plate and incubated overnight. Next, cells were treated with PBS, rhIL2 (0.1 or 1 ng), sEVs (5 μ g), or IL2-sEVs (5 μ g) for 24 h at 37°C. Thereafter, 25 μ l of cell supernatant was collected and incubated with 75 μ l Quanti-Blue reagent (InvivoGen) for 1 h at 37°C. Absorbance at 630 nm was measured using a microplate reader.

4.9 | T cell-mediated cytotoxicity assay

For the MTS assay, 10 μ g of sEV or IL2-sEV-treated B16F10 cells or SK-MEL-28 cells were seeded at the density of $0.5-1 \times 10^5$ cells/ml in a 96-well plate. After 48 h of incubation, the cells were co-cultured with CTLL-2 cells or PBMCs. At the end of the incubation, the MTS reagent was added to each well and incubated for 1 h at 37°C. The absorbance was analysed using a microplate reader at 490 nm. For Luminescence and Fluorescence Animal Imaging System (IVIS) analysis, B16F10-luc-g5 cells were treated with sEVs and D-luciferin (P/N 122799, PerkinElmer) was used as the substrate. Luminescence was analysed using the IVIS software. (Jenkins et al., 2003; Mendel et al., 2003)

4.10 | Flow cytometry

All immune cells were fixed with 4% paraformaldehyde (PFA) in PBS and incubated for 15 min at RT. After washing with PBS, the cells were incubated with primary antibodies for 1 h at 4°C. The cells were then washed with PBS and incubated with secondary antibodies for 30 min at room temperature. The samples were analysed using flow cytometry (Aria III, Becton Dickinson) and the data were analysed using the FlowJo software (BD).

4.11 | Proteomics

All proteomic experimental procedures were performed according to a previous report (Im et al., 2019). Exosomal proteins were digested with trypsin (Cho et al., 2017). The tryptic peptides were analysed using nano-ultra-high-performance LC (UPLC, Waters) and tandem mass spectrometry using a Q-ToF Premier (Waters) (Cho et al., 2012; Moon et al., 2011). The digested peptides were injected into a 2 cm \times 180 μ m trap column and resolved using a 25 cm \times 75 μ m nano ACQUITY C18 column (Waters) on the LC system. All samples were analysed in triplicate. For protein identification, MS raw data were converted into peak lists using MASCOT Distiller version 2.1 (Matrix Science) using the default settings. All MS/MS raw data were analysed using MASCOT version 2.2.1 (Matrix Science). (Cho et al., 2012) The MASCOT was used to search the SwissProt database (release 2018_07) with human taxonomy. Quantification was performed using PEAKS Studio version 10.0 (Bioinformatics Solution Inc.). For label-free protein quantification, the identified peptides were filtered based on a false discovery rate <1%. The abundance of each peptide was determined using ion chromatography extraction and the protein ratio was calculated using the average abundance of the corresponding peptides. Protein ratios were considered acceptable when the proteins contained more than one unique peptide.

4.12 | Small RNA isolation from sEVs

Exosomal RNAs were extracted using TRIzol reagent (Invitrogen) according to the manufacturer's instructions. RNA quality was assessed using an Agilent 2100 bioanalyser with an RNA 6000 Nano Chip (Agilent Technologies, Amstelveen, Netherlands). RNA quantification was performed using a NanoDrop 2000 spectrophotometer (Thermo Fisher Scientific).

4.13 | Small RNA library preparation and sequencing

For control and test RNAs, the library was constructed using the NEBNext Multiplex Small RNA Library Prep kit (New England BioLabs) according to the manufacturer's instructions. For library construction, 3 ng exosomal RNAs from each sample were used to ligate the adaptors and cDNA was synthesized using reverse transcriptase with adaptor-specific primers. PCR was performed for library amplification and libraries were cleaned using a QIAquick PCR purification kit (Qiagen) and AMPure XP beads (Beckman Coulter). The yield and size distribution of the small RNA libraries were assessed with an Agilent 2100 bioanalyser instrument for the high-sensitivity DNA assay (Agilent Technologies). High-throughput sequences were generated using a NextSeq550 system for single-end 75 sequencing (Illumina).

4.14 | Small RNA data analysis

Sequences were mapped using the bowtie2 software tool to obtain a bam file (alignment file). (Langmead & Salzberg, 2012) A mature miRNA sequence was used as a reference for mapping. Read counts mapped onto the mature miRNA sequence were extracted from the alignment file using bed tools (v2.25.0) and Bioconductor that uses the R (version 3.2.2) statistical programming language (R Development Core Team, 2011) (Quinlan & Hall, 2010; Robinson et al., 2010). Read counts were used to determine the expression levels of the miRNAs. The quantile normalization method was used for comparison between samples. miRWalk 2.0 was used to identify genes targeted by the miRNAs.

4.15 | Transfection of miRNA mimics

miRNA mimics or scrambled miRNA (Bioneer, Korea), 100 nM each, were transfected into cells using Lipofectamine™ RNA iMAX transfection reagent (Invitrogen). Cells were incubated at 37°C in a 5% CO₂ atmosphere for 24 or 48 h and harvested with TRIzol reagent (Invitrogen) (Choi et al., 2014; Kang et al., 2013).

4.16 | Immunofluorescence staining and confocal microscopy

Cells were seeded onto glass coverslips at the density of 5×10^4 cells/ml in a two-well confocal chamber, incubated overnight, and treated with sEVs or IL2-sEVs for an additional 48 h. For detection, an antibody was added to the culture medium and incubated for 1 h before fixing with 4% PFA for 10 min at room temperature. The fixed cells were washed with PBS and the coverslips were stained and mounted using a DAPI-containing mounting solution. Immunostaining of 5 μ m thick specimens of O.C.T. compound-embedded fresh frozen cancer tissues was performed using PD-L1, Rab27a, and CD63 antibodies. After fixation with 4% PFA, nonspecific binding was blocked using 5% normal goat serum in PBS for 1 h. The slides were incubated with primary antibodies diluted in 5% normal goat serum (100 μ l/slide) overnight at 4°C. After washing, secondary antibodies were added and incubated for 1 h. The slides were washed again, and the coverslip was stained and mounted using a DAPI-containing mounting solution. Fluorescence images were obtained using an Olympus/FV1200 laser scanning confocal microscope.

4.17 | Studies using syngeneic cancer and xenograft mice models

All animal experiments were performed in accordance with protocols approved by the DGIST Institutional Animal Care and Use Committee (IACUCs, approval number; 19120502-00). For a syngeneic cancer mouse model, B16F10-luc-g5 cells were subcutaneously injected into 7-week-old male wild type (WT) C57BL/6 mice (Orient Bio, Korea). sEVs or IL2-sEVs (20 μ g) were injected intratumourally three times a week for 2 weeks. For the combination therapy approach (Aloulou et al., 2016; Cascio et al., 2021; Legha et al., 1996; Park et al., 2018), cisplatin (Merck, 250 μ g) or α PD-L1 Ab (100 μ g) were intraperitoneally administered for 2 weeks. Tumour growth was measured every 2 days using a caliper. After 2 weeks, the mice were euthanized and luminescence was measured using an IVIS imaging system. For a cancer xenograft model, SK-MEL-28 cells were subcutaneously injected into 7-week-old male CAnN.Cg-Foxn1^{tmu}/Crl mice (Orient Bio, Korea). sEVs or IL2-sEVs (20 μ g) were injected intratumourally for 2 weeks. For studying metastasis, B16F10-luc-g5 cells were intravenously injected three times a week into the mouse tail vein of 7-week-old WT C57BL/6 mice. sEVs or IL2-sEVs (20 μ g) were injected intravenously. Tumour growth was monitored weekly for 2 weeks using an IVIS imaging system (Jenkins et al., 2003; Mendel et al., 2003).

4.18 | Immunohistochemistry

First, 5 μm thick sections of paraffin-embedded cancer tissues were fixed in 4% PFA. After deparaffinization with xylene, the slides were rehydrated with decreasing concentrations of ethanol before washing with PBS. Tissue slides in antigen retrieval buffer (Abcam, ab93678) were boiled for 20 min followed by cooling down at room temperature for 2 h. Hydrogen peroxide (3%) and 5% normal goat serum (Vector Laboratories, S-1000) in PBS were used for blocking peroxidase and non-specific binding, respectively. After washing thrice with PBS, the samples were incubated with the specific primary antibodies against PD-L1, Rab27a, CD3 ϵ , CD8, F4/80, CD11c, or FoxP3 and then with secondary antibodies following the same procedures as used for immunofluorescence staining. The slides were incubated with 200 μl DAB (Vector Laboratories, SK-4100) at room temperature, counterstained with hematoxylin for 1–3 min, and then analysed using a bright-field microscope.

4.19 | Statistical analysis

Statistical analysis was performed using the PRISM 8 software (GraphPad Software, Inc.). All data are presented as the mean \pm standard error of the mean as indicated in the figure legends. If normality was not rejected, t-tests or analyses of covariance were performed. When normality was rejected, Mann–Whitney or Kruskal–Wallis nonparametric tests were used. * $p < 0.05$, ** $p < 0.01$, *** $p < 0.001$, and **** $p < 0.0001$ indicate statistical significance, and p values are further provided in the figure legends. Statistical tests used to determine significance and level of statistical significance for each experiment are indicated in the figure legends.

ACKNOWLEDGEMENTS

We thank the late Prof. Richard A. Lerner for his suggestions regarding the preparation of manuscript. This study was supported by the Bio & Medical Technology Development Program of the National Research Foundation (NRF) of Korea funded by the Korean government (MSIT) (2017M3A9G8083382, 2020M3A9I4039539 and 2019M3A9H1103607), National Research Foundation of Korea (NRF) grant funded by the Korean government (MSIT) (2021R1A5A2021614), DGIST Program of the Ministry of Science and ICT (21-DGRIP-01), and 2020 Joint Research Project of Institutes of Science and Technology and National Cancer Center, Korea (NCC-203205).

AUTHOR CONTRIBUTIONS

Dokyung Jung: Conceptualization; Formal analysis; Investigation; Methodology; Validation; Visualization; Writing – original draft; Writing – review & editing. Sanghee Shin: Data curation; Methodology; Software; Writing – original draft; Writing – review & editing. Inseong Jung: Data curation; Methodology; Software; Validation; Writing – original draft. Suyeon Ryu: Data curation; Methodology; Software; Visualization. Soojeong Noh: Data curation; Methodology; Software; Writing – original draft. Jongwon Jeong: Resources; Software; Validation. Kwang-Soo Kim: Visualization; Writing – original draft. Jong Hyuk Yoon: Software; Validation. Chan-Hyeong Lee: Resources; Software; Validation. Felicitas Bucher: Validation; Writing – original draft; Writing – review & editing. Yong-Nyun Kim: Writing – original draft; Writing – review & editing. Sin-Hyeog Im: Supervision; Validation. Byoung-Joon Song: Supervision; Validation; Writing – review & editing. Kyungmoo Yea: Conceptualization; Funding acquisition; Project administration; Supervision; Writing – original draft; Writing – review & editing.

CONFLICT OF INTEREST

The authors declare no conflict of interest.

ORCID

Dokyung Jung  <https://orcid.org/0000-0002-8502-7370>

Sanghee Shin  <https://orcid.org/0000-0001-8584-8382>

Inseong Jung  <https://orcid.org/0000-0003-3528-2397>

Moon-Chang Baek  <https://orcid.org/0000-0002-4266-1048>

REFERENCES

- Ahmadzadeh, M., & Rosenberg, S. A. (2006). IL-2 administration increases CD4⁺ CD25(hi) Foxp3⁺ regulatory T cells in cancer patients. *Blood*, *107*, 2409–2414.
- Aloulou, M., Carr, E. J., Gador, M., Bignon, A., Libblau, R. S., Fazilleau, N., & Linterman, M. A. (2016). Follicular regulatory T cells can be specific for the immunizing antigen and derive from naive T cells. *Nature communications*, *7*, 1–10.
- Bobrie, A., Krumeich, S., Reyat, F., Recchi, C., Moita, L. F., Seabra, M. C., Ostrowski, M., & Théry, C. (2012). Rab27a supports exosome-dependent and -independent mechanisms that modify the tumour microenvironment and can promote tumour progression. *Cancer Res*, *72*, 4920–4930.
- Boyman, O., & Sprent, J. (2012). The role of interleukin-2 during homeostasis and activation of the immune system. *Nature Reviews Immunology*, *12*, 180–190.
- Bucher, F., Lee, J., Shin, S., Kim, M. S., Oh, Y. S., Ha, S., Zhang, H., & Yea, K. (2018). Interleukin-5 suppresses vascular endothelial growth factor-induced angiogenesis through STAT5 signaling. *Cytokine*, *110*, 397–403.

- Cascio, S., Chandler, C., Zhang, L., Sinno, S., Gao, B., Onkar, S., Bruno, T. C., Vignali, D. A. A., Mahdi, H., Osmanbeyoglu, H. U., Vlad, A. M., & Coffman, L. G. (2021). Buckanovich RJ Cancer-associated MSC drive tumour immune exclusion and resistance to immunotherapy, which can be overcome by Hedgehog inhibition. *Science advances*, 7, eabi5790.
- Chen, G., Huang, A. C., Zhang, W., Zhang, G., Wu, M., Xu, W., Yu, Z., Yang, J., Wang, B., Sun, H., Xia, H., Man, Q., Zhong, W., Antelo, L. F., Wu, B., Xiong, X., Liu, X., Guan, L., Li, T., ... Guo, W. (2018). Exosomal PD-L1 contributes to immunosuppression and is associated with anti-PD-1 response. *Nature*, 560, 382–386.
- Cheng, L., Sun, X., Scicluna, B. J., Coleman, B. M., & Hill, A. F. (2014). Characterization and deep sequencing analysis of exosomal and non-exosomal miRNA in human urine. *Kidney international*, 86, 433–444.
- Cheng, Q., Shi, X., Han, M., Smbatyan, G., Lenz, H. J., & Zhang, Y. (2018). Reprogramming exosomes as nanoscale controllers of cellular immunity. *Journal of the American Chemical Society*, 140, 16413–16417.
- Cho, Y. E., Im, E. J., Moon, P. G., Mezey, E., Song, B. J., & Baek, M. C. (2017). Increased liver-specific proteins in circulating extracellular vesicles as potential biomarkers for drug- and alcohol-induced liver injury. *PLoS one*, 12, e0172463.
- Cho, Y. E., Singh, T. S. K., Lee, H. C., Moon, P. G., Lee, J. E., Lee, M. H., Choi, E. C., Chen, Y. J., Kim, S. H., & Baek, M. C. (2012). In-depth identification of pathways related to cisplatin-induced hepatotoxicity through an integrative method based on an informatics-assisted label-free protein quantitation and microarray gene expression approach. *Molecular & Cellular Proteomics*, 11, .
- Choi, K. Y., Silvestre, O. F., Huang, X., Hida, N., Liu, G., Ho, D. N., Lee, S., Lee, S. W., Hong, J. I., & Chen, X. (2014). A nanoparticle formula for delivering siRNA or miRNAs to tumour cells in cell culture and in vivo. *Nature protocols*, 9, 1900–1915.
- Choudhry, H., Helmi, N., Abdulaal, W. H., Zeyadi, M., Zamzami, M. A., Wu, W., Mahmoud, M. M., Warsi, M. K., Rasool, M., & Jamal, M. S. (2018). Prospects of IL-2 in cancer immunotherapy. *BioMed research international*, 2018, .
- Daassi, D., Mahoney, K. M., & Freeman, G. J. (2020). The importance of exosomal PDL1 in tumour immune evasion. *Nature Reviews Immunology*, 20, 209–215.
- Datta, A., Kim, H., Lal, M., McGee, L., Johnson, A., Moustafa, A. A., Jones, J. C., Mondal, D., & Ferrer, M. (2017). Abdel-Mageed AB. Manumycin A suppresses exosome biogenesis and secretion via targeted inhibition of Ras/Raf/ERK1/2 signaling and hnRNP H1 in castration-resistant prostate cancer cells. *Cancer Lett*, 408, 73–81.
- El, A. S., Mager, I., Breakefield, X. O., & Wood, M. J. (2013). Extracellular vesicles: Biology and emerging therapeutic opportunities. *Nature Reviews Drug Discovery*, 12, 347–357.
- Finney, H. M., Akbar, A. N., & Lawson, A. D. (2004). Activation of resting human primary T cells with chimeric receptors: Costimulation from CD28, inducible costimulator, CD134, and CD137 in series with signals from the TCR ζ chain. *The Journal of Immunology*, 172, 104–113.
- Fu, W., Lei, C., Liu, S., Cui, Y., Wang, C., Qian, K., Li, T., Shen, Y., Fan, X., Lin, F., Ding, M., Pan, M., Ye, X., Yang, Y., & Hu, S. (2019). CAR exosomes derived from effector CAR-T cells have potent antitumour effects and low toxicity. *Nature communications*, 10, 1–12.
- Gangadaran, P., & Ahn, B. - C. (2020). Extracellular vesicle- and extracellular vesicle mimetics-based drug delivery systems: New perspectives, challenges, and clinical developments. *Pharmaceutics*, 12, 442.
- Herrmann, I. K., Wood, M. J. A., & Fuhrmann, G. (2021). Extracellular vesicles as a next-generation drug delivery platform. *Nature nanotechnology*, 16, 748–759.
- Hokland, P., & Heron, I. (1980). The Isopaque–Ficoll Method Re-evaluated: Selective Loss of Autologous Rosette-forming Lymphocytes during Isolation of Mononuclear Cells from Human Peripheral Blood. *Scandinavian journal of immunology*, 11, 353–356.
- Huang, X., Yuan, T., Tschannen, M., Sun, Z., Jacob, H., Du, M., Liang, M., Dittmar, R. L., Liu, Y., Liang, M., Kohli, M., Thibodeau, S. N., Boardman, L., & Wang, L. (2013). Characterization of human plasma-derived exosomal RNAs by deep sequencing. *BMC genomics*, 14, 1–14.
- Im, E. J., Lee, C. H., Moon, P. G., Rangaswamy, G. G., Lee, B., Lee, J. M., Lee, J. C., Jee, J. G., Bae, J. S., Kwon, T. K., Kang, K. W., Jeong, M. S., Lee, J. E., Jung, H. S., Ro, H. J., Jun, S., Kang, W., Seo, S. Y., Cho, Y. E., ... Baek, M. C. (2019). Sulfisoxazole inhibits the secretion of small extracellular vesicles by targeting the endothelin receptor A. *Nature Communications*, 10, 1387.
- Jenkins, D. E., Oei, Y., Hornig, Y. S., Yu, S. F., Dusich, J., Purchio, T., & Contag, P. R. (2003). Bioluminescent imaging (BLI) to improve and refine traditional murine models of tumour growth and metastasis. *Clinical & experimental metastasis*, 20, 733–744.
- Jiang, T., Zhou, C., & Ren, S. (2016). Role of IL-2 in cancer immunotherapy. *Oncoimmunology*, 5, e1163462.
- Kaiser, J. (2016). Malignant messengers. *Science*, 352, 164–166.
- Kalantari Khandani, N., Ghahremanloo, A., & Hashemy, S. I. (2020). Role of tumour microenvironment in the regulation of PD-L1: A novel role in resistance to cancer immunotherapy. *Journal of cellular physiology*, 235, 6496–6506.
- Kang, S.-M., Lee, H.-J., & Cho, J.-Y. (2013). MicroRNA-365 regulates NKX2-1, a key mediator of lung cancer. *Cancer letters*, 335, 487–494.
- Koh, E., Lee, E. J., Nam, G. H., Hong, Y., Cho, E., Yang, Y., & Kim, I. S. (2017). Exosome-SIR α , a CD47 blockade increases cancer cell phagocytosis. *Biomaterials*, 121, 121–129.
- Langmead, B., & Salzberg, S. L. (2012). Fast gapped-read alignment with Bowtie 2. *Nature methods*, 9, 357–359.
- Legha, S. S., Ring, S., Bedikian, A., Plager, C., Eton, O., Buzaid, A. C., & Papadopoulos, N. (1996). Treatment of metastatic melanoma with combined chemotherapy containing cisplatin, vinblastine and dacarbazine (CVD) and biotherapy using interleukin-2 and interferon- α . *Annals of oncology*, 7, 827–835.
- Li, Q. J., Chau, J., Ebert, P. J., Sylvester, G., Min, H., Liu, G., Braich, R., Manoharan, M., Soutschek, J., Skare, P., Klein, L. O., Davis, M. M., & Chen, C. Z. (2007). miR-181a is an intrinsic modulator of T cell sensitivity and selection. *Cell*, 129, 147–161.
- Liang, G., Zhu, Y., Ali, D. J., Tian, T., Xu, H., Si, K., Sun, B., Chen, B., & Xiao, Z. (2020). Engineered exosomes for targeted co-delivery of miR-21 inhibitor and chemotherapeutics to reverse drug resistance in colon cancer. *Journal of Nanobiotechnology*, 18, 10.
- Liu, C., Li, N., & Liu, G. (2020). The role of microRNAs in regulatory T cells. *Journal of Immunology Research*, 2020, .
- Liu, W., Putnam, A. L., Xu-Yu, Z., Szot, G. L., Lee, M. R., Zhu, S., Gottlieb, P. A., Kapranov, P., Gingeras, T. R., Fazekas de, S. G. B., Clayberger, C., Soper, D. M., Ziegler, S. F., & Bluestone, J. A. (2006). CD127 expression inversely correlates with FoxP3 and suppressive function of human CD4+ T reg cells. *The Journal of experimental medicine*, 203, 1701–1711.
- Lu, J., Wu, J., Xie, F., Tian, J., Tang, X., Guo, H., Ma, J., Xu, P., Mao, L., Xu, H., & Wang, S. (2019). CD4(+) T Cell-Released Extracellular Vesicles Potentiate the Efficacy of the HBsAg Vaccine by Enhancing B Cell Responses. *Advanced Science (Weinh)*, 6, 1802219.
- Luan, X., Sansanaphongpricha, K., Myers, I., Chen, H., Yuan, H., & Sun, D. (2017). Engineering exosomes as refined biological nanoplatfoms for drug delivery. *Acta Pharmacologica Sinica*, 38, 754–763.
- Marar, C., Starich, B., & Wirtz, D. (2021). Extracellular vesicles in immunomodulation and tumour progression. *Nature Immunology*, 22, 560–570.
- Mendel, D. B., Laird, A. D., Xin, X., Louie, S. G., Christensen, J. G., Li, G., Schreck, R. E., Abrams, T. J., Ngai, T. J., Lee, L. B., Murray, L. J., Carver, J., Chan, E., Moss, K. G., Haznedar, J. O., Sukbuntherng, J., Blake, R. A., Sun, L., Tang, C., ... Cherrington, J. M. (2003). In vivo antitumour activity of SU11248, a novel tyrosine kinase inhibitor targeting vascular endothelial growth factor and platelet-derived growth factor receptors: Determination of a pharmacokinetic/pharmacodynamic relationship. *Clinical cancer research*, 9, 327–337.

- Mittal, S., Gupta, P., Chaluvally-Raghavan, P., & Pradeep, S. (2020). Emerging Role of Extracellular Vesicles in Immune Regulation and Cancer Progression. *Cancers (Basel)*, *12*, .
- Moon, P. G., Lee, J. E., You, S., Kim, T. K., Cho, J. H., Kim, I. S., Kwon, T. H., Kim, C. D., Park, S. H., Hwang, D., Kim, Y. L., & Baek, M. C. (2011). Proteomic analysis of urinary exosomes from patients of early IgA nephropathy and thin basement membrane nephropathy. *Proteomics*, *11*, 2459–2475.
- Muller, L., Simms, P., Hong, C. S., Nishimura, M. I., Jackson, E. K., Watkins, S. C., & Whiteside, T. L. (2017). Human tumour-derived exosomes (TEX) regulate Treg functions via cell surface signaling rather than uptake mechanisms. *Oncoimmunology*, *6*, e1261243.
- Noman, M. Z., Parpal, S., Van Moer, K., Xiao, M., Yu, Y., Viklund, J., De Milito, A., Hasmim, M., Andersson, M., Amaravadi, R. K., Martinsson, J., Berchem, G., & Janji, B. (2020). Inhibition of Vps34 reprograms cold into hot inflamed tumours and improves anti-PD-1/PD-L1 immunotherapy. *Science Advances*, *6*, eaax7881.
- Park, Y. J., Kuen, D. S., & Chung, Y. (2018). Future prospects of immune checkpoint blockade in cancer: From response prediction to overcoming resistance. *Experimental & Molecular Medicine*, *50*, 109.
- Pectasides, D., Yianniotis, H., Alevizakos, N., Bafaloukos, D., Barbounis, V., Varthalitis, J., Dimitriadis, M., & Athanassiou, A. (1989). Treatment of metastatic malignant melanoma with dacarbazine, vindesine and cisplatin. *British journal of cancer*, *60*, 627–629.
- Peinado, H., Alečković, M., Lavotshkin, S., Matei, I., Costa-Silva, B., Moreno-Bueno, G., Hergueta-Redondo, M., Williams, C., Garcia-Santos, G., Ghajar, C., Ntitoro-Hoshino, A., Hoffman, C., Badal, K., Garcia, B. A., Callahan, M. K., Yuan, J., Martins, V. R., Skog, J., Kaplan, R. N., ... Lyden, D. (2012). Melanoma exosomes educate bone marrow progenitor cells toward a pro-metastatic phenotype through MET. *Nature Medicine*, *18*, 883–891.
- Pitt, J. M., Charrier, M., Viaud, S., André, F., Besse, B., Chaput, N., & Zitvogel, L. (2014). Dendritic cell-derived exosomes as immunotherapies in the fight against cancer. *The Journal of Immunology*, *193*, 1006–1011.
- Poggio, M., Hu, T., Pai, C. C., Chu, B., Belair, C. D., Chang, A., Montabana, E., Lang, U. E., Fu, Q., & Fong, L. (2019). Bcl-2 Induced Suppression of Exosomal PD-L1 Induces Systemic Anti-tumour Immunity and Memory. *Cell*, *177*, 414–427e413.
- Quinlan, A. R., & Hall, I. M. (2010). BEDTools: A flexible suite of utilities for comparing genomic features. *Bioinformatics*, *26*, 841–842.
- Read, S., Malmström, V., & Powrie, F. (2000). Cytotoxic T lymphocyte-associated antigen 4 plays an essential role in the function of CD25+ CD4+ regulatory cells that control intestinal inflammation. *The Journal of experimental medicine*, *192*, 295–302.
- Robinson, M. D., McCarthy, D. J., & Smyth, G. K. (2010). edgeR: A Bioconductor package for differential expression analysis of digital gene expression data. *Bioinformatics*, *26*, 139–140.
- Romeu, M. A., Mestre, M., González, L., Valls, A., Verdager, J., Corominas, M., Bas, J., Massip, E., & Buendia, E. (1992). Lymphocyte immunophenotyping by flow cytometry in normal adults. Comparison of fresh whole blood lysis technique, Ficoll-Paque separation and cryopreservation. *Journal of immunological methods*, *154*, 7–10.
- Seo, N., Shirakura, Y., Tahara, Y., Momose, F., Harada, N., Ikeda, H., Akiyoshi, K., & Shiku, H. (2018). Activated CD8+ T cell extracellular vesicles prevent tumour progression by targeting of lesional mesenchymal cells. *Nature communications*, *9*, 1–11.
- Sheehan, C., & D'Souza-Schorey, C. (2019). Tumour-derived extracellular vesicles: Molecular parcels that enable regulation of the immune response in cancer. *J Cell Sci*, *132*, .
- Soengas, M. S., & Lowe, S. W. (2003). Apoptosis and melanoma chemoresistance. *Oncogene*, *22*, 3138–3151.
- Spolski, R., Li, P., & Leonard, W. J. (2018). Biology and regulation of IL-2: From molecular mechanisms to human therapy. *Nature Reviews Immunology*, *18*, 648–659.
- Stathopoulou, C., Gangaplara, A., Mallett, G., Flomerfelt, F. A., Liniany, L. P., Knight, D., Samsel, L. A., Berlinguer-Palmini, R., Yim, J. J., Felizardo, T. C., Eckhaus, M. A., Edgington-Mitchell, L., Martinez-Fabregas, J., Zhu, J., Fowler, D. H., van Kasteren, S. I., Laurence, A., Bogyo, M., Watts, C., ... Amarnath, S. (2018). PD-1 inhibitory receptor downregulates asparaginyl endopeptidase and maintains Foxp3 transcription factor stability in induced regulatory T cells. *Immunity*, *49*, 247–263e247.
- Stockis, J., Colau, D., Coulie, P. G., & Lucas, S. (2009). Membrane protein GARP is a receptor for latent TGF- β on the surface of activated human Treg. *European journal of immunology*, *39*, 3315–3322.
- Szajnik, M., Czystowska, M., Szczepanski, M. J., Mandapathil, M., & Whiteside, T. L. (2010). Tumour-derived microvesicles induce, expand and up-regulate biological activities of human regulatory T cells (Treg). *PloS one*, *5*, e11469.
- Thery, C., Zitvogel, L., & Amigorena, S. (2002). Exosomes: Composition, biogenesis and function. *Nature Reviews Immunology*, *2*, 569–579.
- Tian, Y., Zhang, F., Qiu, Y., Wang, S., Li, F., Zhao, J., Pan, C., Tao, Y., Yu, D., & Wei, W. (2021). Reduction of choroidal neovascularization via cleavable VEGF antibodies conjugated to exosomes derived from regulatory T cells. *Nature Biomedical Engineering*, *5*, 968–982.
- Torralba, D., Baixauli, F., Villarroya-Beltri, C., Fernández-Delgado, I., Latorre-Pellicer, A., Acín-Pérez, R., Martín-Cófreces, N. B., Ál, J.-T., Iborra, S., Jorge, I., González-Aseguinolaza, G., Garaude, J., Vicente-Manzanares, M., Enríquez, J. A., Mittelbrunn, M., & Sánchez-Madrid, F. (2018). Priming of dendritic cells by DNA-containing extracellular vesicles from activated T cells through antigen-driven contacts. *Nature Communications*, *9*, 2658.
- Van Der Vlist, E. J., Nolte, E. N., Stoorvogel, W., Arksteijn, G. J., & Wauben, M. H. (2012). Fluorescent labeling of nano-sized vesicles released by cells and subsequent quantitative and qualitative analysis by high-resolution flow cytometry. *Nature protocols*, *7*, 1311–1326.
- Wang, X., Xiang, Z., Liu, Y., Huang, C., Pei, Y., Wang, X., Zhi, H., Wong, W. H., Wei, H., Ng, I. O., Lee, P. P., Chan, G. C., Lau, Y. L., & Tu, W. (2020). Exosomes derived from V δ 2-T cells control Epstein-Barr virus-associated tumours and induce T cell antitumour immunity. *Science Translational Medicine*, *12*, eaaz3426.
- Wiklander, O. P., Brennan, M. Á., Lötvall, J., Breakefield, X. O., & El Andaloussi, S. (2019). Advances in therapeutic applications of extracellular vesicles. *Science translational medicine*, *11*, eaav8521.
- Xie, F., Xu, M., Lu, J., Mao, L., & Wang, S. (2019). The role of exosomal PD-L1 in tumour progression and immunotherapy. *Molecular Cancer*, *18*, 146.
- Xu, R., Greening, D. W., Rai, A., Ji, H., & Simpson, R. J. (2015). Highly-purified exosomes and shed microvesicles isolated from the human colon cancer cell line LIM1863 by sequential centrifugal ultrafiltration are biochemically and functionally distinct. *Methods*, *87*, 11–25.
- Yan, W., & Jiang, S. (2020). Immune Cell-Derived Exosomes in the Cancer-Immunity Cycle. *Trends Cancer*, *6*, 506–517.
- Yang, E., Wang, X., Gong, Z., Yu, M., Wu, H., & Zhang, D. (2020). Exosome-mediated metabolic reprogramming: The emerging role in tumour microenvironment remodeling and its influence on cancer progression. *Signal Transduct Target Ther*, *5*, 242.
- Zerial, M., & McBride, H. (2001). Rab proteins as membrane organizers. *Nature reviews Molecular cell biology*, *2*, 107–117.
- Zha, Z., Bucher, F., Nejatfard, A., Zheng, T., Zhang, H., Yea, K., & Lerner, R. A. (2017). Interferon- γ is a master checkpoint regulator of cytokine-induced differentiation. *Proceedings of the National Academy of Sciences*, *114*, E6867–E6874.
- Zhang, J., Yamada, O., Kida, S., Murase, S., Hattori, T., Oshima, Y., & Kikuchi, H. (2020). Downregulation of PD-L1 via amide analogues of brefelamide: Alternatives to antibody-based cancer immunotherapy. *Experimental and therapeutic medicine*, *19*, 3150–3158.

SUPPORTING INFORMATION

Additional supporting information can be found online in the Supporting Information section at the end of this article.

How to cite this article: Jung, D., Shin, S., Kang, S.-M., Jung, I., Ryu, S., Noh, S., Choi, S.-J., Jeong, J., Lee, B. Y., Kim, K.-S., Kim, C. S., Yoon, J. H., Lee, C.-H., Bucher, F., Kim, Y.-N., Im, S.-H., Song, B.-J., Yea, K., & Baek, M.-C. (2022). Reprogramming of T cell-derived small extracellular vesicles using IL2 surface engineering induces potent anti-cancer effects through miRNA delivery. *Journal of Extracellular Vesicles*, 11, e12287. <https://doi.org/10.1002/jev2.12287>